ACS OMEGA

http://pubs.acs.org/journal/acsodf

Article

A Structural Network Analysis of Neuronal ArhGAP21/23 Interactors by Computational Modeling

Zen Kouchi* and Masaki Kojima

Cite This: *ACS Omega* 2023, 8, 19249−19264

Read Online

ACCESS | Metrics & More | Article Recommendations | Supporting Information

ABSTRACT: RhoGTPase-activating proteins (RhoGAPs) play multiple roles in neuronal development; however, details of their substrate recognition system remain elusive. ArhGAP21 and ArhGAP23 are RhoGAPs that contain N-terminal PDZ and pleckstrin homology domains. In the present study, the RhoGAP domain of these ArhGAPs was computationally modeled by template-based methods and the AlphaFold2 software program, and their intrinsic RhoGTPase recognition mechanism was analyzed from the domain structures using the protein docking programs HADDOCK and HDOCK. ArhGAP21 was predicted to preferentially catalyze Cdc42, RhoA, RhoB, RhoC, and RhoG and to downregulate RhoD and Tc10 activities. Regarding ArhGAP23, RhoA and Cdc42 were deduced to be its substrates, whereas RhoD downregulation was predicted to be less efficient. The PDZ domains of ArhGAP21/23 possess the FTLRXXXVY sequence, and similar globular folding consists of antiparalleled β-sheets and two α-helices that are conserved with PDZ domains of MAST-family proteins. A peptide docking analysis revealed the specific interaction of the ArhGAP23 PDZ domain with the PTEN C-terminus. The pleckstrin homology domain structure of ArhGAP23 was also predicted, and the functional selectivity for the interactors regulated by the folding and disordered domains in ArhGAP21 and ArhGAP23 was examined by an *in silico* analysis. An interaction analysis of these RhoGAPs revealed the existence of mammalian ArhGAP21/23-specific type I and type III Arf- and RhoGTPase-regulated signaling. Multiple recognition systems of RhoGTPase substrates and selective Arf-dependent localization of ArhGAP21/23 may form the basis of the functional core signaling necessary for synaptic homeostasis and axon/dendritic transport regulated by RhoGAP localization and activities.

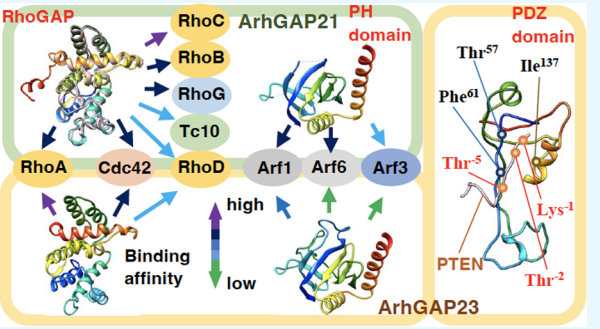

INTRODUCTION

The regulation of mammalian RhoGTPase functions in neuronal development is a highly organized process, and the dysfunction of these elements causes several developmental disorders. RhoGTPases are regulated by RhoGTPase-activating proteins (RhoGAPs), Rho guanine dissociation inhibitors (RhoGDIs), and Rho guanine nucleotide exchange factors (RhoGEFs), which spatiotemporally regulate GTP-hydrolyzing activities and GTP/GDP exchange reactions. RhoGAPs regulate cellular morphology and the synaptic network; however, the details of the signaling cross talk events involved in their activation during the developmental process remain unclear.[1]

Mutations in RhoGAPs lead to developmental disorders, such as intellectual disability (ID), and specific inhibitors of RhoGTPase regulation have recently been developed for the pharmacological treatment of dysfunctional behavior.[2] Oligophrenin-1 is an X-linked gene whose mutation leads to ID with epileptic phenotypes and morphological phenotypes, including ventricular enlargement; furthermore, the PH-domain containing RhoGAP is highly expressed in the hippocampus and cortex.[3] Several other RhoGAPs, such as ArhGAP21, are enriched in the developmental brain, and exome sequencing of consanguineous families with neurogenetic developmental disorders, including brain malformation, has revealed rare single nucleotide variants in the homozygous ArhGAP21 locus.[4] A genome-wide association study of reading disabilities has shown candidate single nucleotide polymorphisms in the *ArhGAP23* gene to be significantly associated with neurodevelopmental disorders.[5]

Both ArhGAP21 and ArhGAP23 comprise the N-terminal PDZ domain and RhoGAP domain connected to the PH domain, the splicing isoforms with or without the RhoGAP domain, and the C-terminal disordered domain. Several biochemical and cellular studies have suggested that ArhGAP21 and ArhGAP23 are differently regulated by interactors, and a protein interaction database developed based on results of high-throughput studies shows distinct sets

Received: December 19, 2022
Accepted: May 5, 2023
Published: May 23, 2023

of profiles of their complexes.[6] ArhGAP21 specifically binds GTP-bound forms of Arf1 and Arf6 and regulates actin organization in the Golgi apparatus.[7,8] β-Arrestin 1 attenuates ArhGAP21-mediated RhoGAP activity through the angiotensin II receptor following angiotensin treatment.[9] ArhGAP23 is homologous to ArhGAP21 and interacts with Prickle1 for the regulation of lateral signaling and Rho activation during cancer invasion.[10] A phenotypic analysis of heterozygous ArhGAP21 knockout mice has revealed various functions of this protein as a regulator of lineage-specification of stem cell populations.[11,12] In contrast, the physiological function of ArhGAP23 remains unknown.[13]

The neuronal functions of both ArhGAP21 and ArhGAP23 proteins are suggested to be associated with neuronal scaffold interactors and modulators of the metabotropic glutamate receptor (mGluR) function.[14,15] A stage-specific analysis of synaptic development revealed that ArhGAP23 plays an important role in promoting spinal maturation.[16] A proteomic analysis of serotonin transporter interactors regulated by 5-HT signaling also indicated the involvement of ArhGAP21 and ArhGAP23 in the serotonin signaling pathway.[17] The expression of ArhGAP21 and ArhGAP23 in the cortex and hippocampus tends to change similarly during the prenatal and postnatal developmental stages, and both have been shown to be localized with postsynaptic density within excitatory glutamatergic neurons, suggesting the existence of a common regulatory pathway, at least partially, for both proteins.[18] The expression of ArhGAP21 and ArhGAP23 is cooperatively regulated in a tissue-specific manner.[19]

We therefore examined the substrate specificity of the mammalian PDZ-containing RhoGAPs and their specific interactors based on predicted structural aspects as most RhoGAPs do not show any selectivity toward a particular RhoGTPase, in contrast to Dbl-family proteins, which show selective RhoGEF activities toward Rho, Cdc42, and Rac proteins *via* specific residues.[20] In particular, the difference in the substrate recognition mechanism of RhoGAP domains between ArhGAP21 and ArhGAP23 remains unclear, although both RhoGAP domains possess highly homologous sequences with each other. The Arf-binding regions, including the PH domains of ArhGAP21, are postulated to interact with Arf-subfamily proteins, but no structural information on ArhGAP23 has been reported.

In the present study, prediction of these domains was performed by structural homology modeling and the AlphFold2 software program,[21] and computational peptide interacting mapping was attempted to functionally elucidate the unexplored PDZ domains of ArhGAP21 and ArhGAP23. The predicted mode of these ArhGAP-mediated signaling pathways will be useful for further analyses of their physiological functions.

METHODS

Homology Modeling. Sequences of the RhoGAP and PH domain with the external C-terminal region of ArhGAP21 and ArhGAP23 (Table S1) were submitted for the HHpred detection of secondary structural homology,[22] and multiple alignment-based detection was conducted with a SWISS-MODEL search, taking into account the target-template secondary structure similarity.[23] A suitable model was sought with trRosetta and I-Tasser, which rank top in the Critical Assessment of Techniques for Protein Structure Prediction (CASP) for checking potential templates.[24,25] The RhoGAP domains of ArhGAP23 and ArhGAP21 with external C-terminal amino acids were modeled by SWISS-MODEL and trRosetta, respectively, and the candidate model was selected by a quality check. The model quality was estimated with trRosetta, I-Tasser, and QMean, and each structure was visualized using the Chimera software program.[24−26] The predicted model was evaluated by PROCHECK, ERRAT,[27] verify3D,[28] and PROSA[29] (Tables S2 and S3).

Sequence and Structural Analyses of PDZ Domains. Sequences from the PDZ domain of human ArhGAP21 and ArhGAP23, categorized by InterPro,[30] were examined by a PSI-BLAST[31] search by restricting RefSeq to *Homo sapiens*. The PSI-BLAST search identified multiple members belonging to the microtubule-associated serine/threonine protein kinase (MAST) and membrane-associated guanylate kinase (MAGI) family of proteins with high-ranked matching scores. Their sequences were aligned using the MAFFT software program,[32] and the tertiary structure was analyzed using the PDB website.

Molecular Docking. A modeled ArhGAP21 or ArhGAP23 Rho-GTPase docking analysis was performed by HDOCK in hybrid-docking or template-free docking mode for selection.[33] The HADDOCK program was also conducted based on the known PDB structure.[34] The interatom energies and side chains of modeled domain structures were optimized by the EGAD software program.[35] The ability of these programs to reproduce the RhoA-RhoGAP interaction was checked by the HDOCK or HADDOCK flexible hybrid-docking performing program for MgcRacGAP (PDB codes: 5c2k and 5c2j) or modeled complex N-chimerin-RhoGAP (PDB code: 3cxl, Figure S1) with Rac1 that showed a similar tertiary structure toward each RhoGTPase .[33,34] Interactions of the RhoGAP domain and Arf binding domain (ArfBD), including the PH domain, with RhoGTPase family and Arf-family proteins were modeled using HADDOCK by *ab initio* docking with the experimental constraints on the conserved residues in the interface with analogy to conserved catalytic arginine and the ArfBD[7] (PDB code: 2dhj) based on the selected structural model, respectively.[34] The following conserved residues were used for the HADDOCK analysis: the catalytic Arg^{1183} and Pro^{1185} residues for the RhoGAP domain of ArhGAP21; the Arg^{942} and Pro^{944} residues for the RhoGAP domain of ArhGAP23; the conserved Tyr^{999}, Ser^{1000}, Ile^{1053}, and Ile^{1057} residues for the ArhGAP21 ArfBD; and the Tyr^{767}, Ser^{768}, and Ile^{822} residues for the ArhGAP23 ArfBD. HDOCK was also used to determine the prediction and selectivity of RhoGAP substrates. Interaction residues of Rho-family proteins that located in the p-loop, switch I, switch II, and α3-helix are important for the association with RhoGAP; they were identified in elements located <6 Å from conformational aspects. The complex was not selected if the candidate complex did not meet the constraints described in HADDOCK. The complexes retrieved from the PDB database (3msx, 1f7c, 1grn, or 5jcp) were also modeled using the HDOCK software program (Table S4). Regarding the ArfBDs, complexes selected using both the Haddock and HDOCK docking programs were matched well to the crystallographic model of the ArhGAP21-Arf1 complex.[7] Computational docking with the ligand peptide was performed by template docking with the MOE system (Chemical Computing Group ULC, Canada). First, MAST2-PDZ complexed with the C-terminus of PTEN (PDB code: 2kyl) was used as a template. After matching its position to the ArhGAP-PDZ structures modeled by UCSF Chimera, the PTEN moiety was extracted

https://doi.org/10.1021/acsomega.2c08054
ACS Omega 2023, 8, 19249−19264

from the MAST2-PDZ complex and merged into ArhGAP-PDZ. The initial structure of ArhGAP-PDZ with PTEN was then preprocessed with the QuickPrep tool, and the general docking procedure of MOE was applied to optimize the complex structure. The predicted model was further evaluated using the DrugScorePPI software program to search for critical residues that mediate the protein−protein interfaces by calculating the predicted charges in the binding free energy upon alanine mutations *in silico*.[36] The binding affinity of the predicted complexes was also examined by protein binding energy prediction using PRODIGY with their tertiary structures[37,38] (Table 1). The structure models predicted by the AlphaFold2 software program were also used to predict the complex structures of ArhGAP21 and ArhGAP23s.[21] The RhoGAP domain of ArhGAP21 with external C-terminal amino acids was also modeled using the AlphaFold2 software program and analyzed by the HDOCK and Haddock software programs.

Table 1. Binding Affinity of Interactors to ArhGAP21 and ArhGAP23 RhoGAPs[a]

RhoGAP domain	ΔG (kcal/mol)	theoretical K_D (M)
ArhGAP21		
Cdc42	−10.1 ± 0.082	8.2e-08 (7.2−9.4e-08)
RhoA	−11.3 ± 0.083	1.1e-08 (0.95−1.2e-08)
RhoB	−10.8 ± 0.087	2.3e-08 (2.0−2.7e-08)
RhoC	−11.5 ± 0.081	7.6e-09 (6.7−8.7e-09)
RhoD	−7.9 ± 0.070	2.5e-06 (2.2−2.8e-06)
RhoG	−11.3 ± 0.074	1.0e-08 (0.93−1.2e-08)
Tc10	−7.9 ± 0.063	2.7e-06 (2.4−3.0e-06)
ArhGAP23		
Cdc42	−10.0 ± 0.084	9.6e-08 (8.4−11e-08)
RhoA	−12.0 ± 0.086	3.3e-09 (2.9−3.8e-09)
RhoD	−7.8 ± 0.069	3.2e-06 (2.9−3.6e-06)
PDB		
5c2j	−10.3 ± 0.085	5.5e-08 (4.8−6.3e-08)
1grn	−9.3 ± 0.083	2.7e-07 (2.4−3.1e-07)
1tx4	−8.9 ± 0.078	5.4e-07 (4.8−6.2e-07)
PH domain	ΔG (kcal/mol)	Theoretical K_D (M)
ArhGAP21		
Arf1 (theoretical value)	−10.5 ± 0.062	4.0e-08 (3.6−4.5e-08)
Arf3	−8.4 ± 0.055	1.3e-06 (1.2−1.4e-06)
Arf6	−10.9 ± 0.061	2.2e-08 (2.0−2.5e-08)
ArhGAP23		
Arf1	−9.3 ± 0.065	2.8e-07 (2.5−3.1e-07)
Arf3	−7.1 ± 0.057	1.1e-05 (0.96−1.2e-05)
Arf6	−7.1 ± 0.057	1.1e-05 (0.96−1.2e-05)
PDZ domain	ΔG (kcal/mol)	theoretical K_D (M)
ArhGAP23		
PTEN	−7.3 ± 0.069	6.8e-06 (6.1−7.6e-06)

[a]Selected models of RhoGAP-RhoGTPase complexes and pleckstrin-homology domains interacting with Arf1, Arf3, and Arf6 were analyzed using the PRODIGY software program with contact-based prediction of binding affinity in protein complexes.[37,38] The binding affinity of the RhoGAP complexes retrieved from the PDB database (PDB codes: 5c2j, 1grn, or 1tx4) was calculated and is shown in the column. Regarding the calculation of estimated errors of Gibbs free energy ($\Delta G = RT \ln K_D$), the standard deviation of the weights in the linear equation (ΔG_{calc} = 0.09459 $IC_{scharged/charged}$ + 0.10007 $IC_{scharged/apolar}$ − 0.19577 $IC_{spolar/polar}$ + 0.22671 $IC_{spolar/apolar}$ − 0.18681%NIS_{apolar} − 0.13810%$NIS_{charged}$ + 15.9433, NIS: non-interacting interface) was considered.[38] The theoretical value of selected models of ArhGAP21 ArfBD interacting with Arf1 by the HADDOCK software program is also shown as Arf1 (theoretical K_D) in the table.

Known ArhGAP21/23 Interaction Analysis and Interactor Prediction. The BioGrid and IntAct databases were used to compile a list of experimentally analyzed ArhGAP21 and ArhGAP23 interactors as well as those manually curated from the literature.[39,40] The binding proteins were annotated with the domain signatures and biological processes involved in physiological aspects by retrieving them from the UniProt InterPro. Details concerning the interaction were also inferred from PubMed results based on selected keywords concerning the neuronal function. The analyzed proteins are indicated by their UniProt accession code in Table S5. To predict potential interactors of ArhGAP21 and ArhGAP23, we searched for putative domains and linear motifs putatively mediating the interactions involved in Arf-mediated signaling in common cell-based models or neurodevelopmental processes. We suspected that a predicted linear motif might be potential interaction sites for a novel interactor if the known binding protein was categorized into a class of protein or contained the motifs known to bind to the corresponding sequences (Table 2).

RESULTS AND DISCUSSION

Substrate Specificity of the RhoGAP Domains of ArhGAP Proteins. ArhGAP21 and ArhGAP23 possess a similar domain organization, both containing PH and PDZ domains. Although their functional redundancy and mutual regulation of expression have been reported in a cell-specific manner, their substrate specificity has remained to be elusive.[8,10,41,42] To investigate the structural determinants of RhoGAP domains in the catalytic reaction, the RhoGAP domains of ArhGAP21 and ArhGAP23 were retrieved from InterPro and modeled based on the predicted secondary structure from HHPred (Figure 1a). The RhoGAP sequences showed 74.6% homology with each other, and the prediction using SWISS-MODEL, trRosetta, and I-Tasser selected ArhGAP2 (PDB code: 3cxl) for ArhGAP21 and ArhGAP2 (PDB code: 3cxl) and MgcRacGAP (PDB code: 5c2k) for ArhGAP23[23−25,32] (Figure 1b, Table S1, Figure S2a,b). All of the models were evaluated based on the Ramachandran plot using PROCHECK and internal nonbonded interactions using ERRAT[27] (Tables S2 and S3). The models were also examined by verify3D, which indicates statistical preference on residues defined by three factors: the conformational buried residue area inaccessible to the solvent, the area fraction of the side-chain area covered by polar atoms, and the local secondary structure. The PROSA software program was used to evaluate the distance-based pair potential and structural quality of the model[29] (Table S2). ArhGAP2 was selected for model prediction for ArhGAP21 and ArhGAP23 (Table S2). The QMean score of the predicted RhoGAP domains was 0.75 for both ArhGAP21 and ArhGAP23 with high reliability.[26] Furthermore, the predicted RhoGAP structures were superimposed onto the RhoGAP domain of the ArhGAP2 template, showing a completely matched helix orientation (Figure S2a,b; Table S1). The RhoGAP domains of ArhGAP21 and ArhGAP23 had the same structural folding in the superimposed orientation (RMSD: 0.058 Å) (Figure 1c). The RhoGAP domains of ArhGAP21, ArhGAP23, and RhoGAP19D retrieved from InterPro were also modeled (Figure 1d) using the AlphaFold2 software program, and the two human RhoGAP domains showed

https://doi.org/10.1021/acsomega.2c08054
ACS Omega 2023, 8, 19249−19264

Table 2. List of Known and Predicted ArhGAP21 and ArhGAP23 Interactors[a]

RhoGAP	interactor	domain architecture	signaling pathway	experimental condition	ref.	interacting region
ArhGAP21	Arf1	Arf domain	dynein and Cdc42 recruitment to Golgi	crystallization	7	Arf binding domain
ArhGAP21	Arf6	Arf domain	regulation of F-actin dynamics, Golgi complex organization	YTH,[b] GST pull-down	8	929−1096aa (PH domain including C-terminal region)
ArhGAP21,23	SERT	transmembrane protein	serotonin transporter	affinity capture MS	17	N.D. (no interaction in SERT knockout mouse)
ArhGAP21	FAK	kinase	integrin signaling, neurite outgrowth, long-term potentiation	immunoprecipitation	83	N.D.
ArhGAP21	YWHAS	14-3-3	cell-cycle arrest	MudPIT analysis[c]	64	Ser671
ArhGAP21	Ank3	ankyrin repeat	assembly of axon initial segment	proximity biotinylation analysis	67	N.D.
ArhGAP21	β-arrestin1 (ARRB1)	arrestin domain	G-protein-coupled signaling, cytoskeletal organization	YTH,[b] peptide binding	9	1332−1356aa (IQHHDW∼VQEEST)
ArhGAP21	α-tubulin	tubulin	cell−cell adhesion epithelial−mesenchymal transition	immunoprecipitation	82	N.D.
ArhGAP21	Graf1	SH3, RhoRAP domain	integrin signaling	proximity biotinylation analysis	84	N.D.
ArhGAP21	NPRAP	coiled-coil, PDZ	synaptic adherens junction	immunoprecipitation	72	N.D.
ArhGAP23	YWHAH	14-3-3	neuronal PKA signaling	affinity purification tag	65	N.D.
ArhGAP23	Prickle1	PET, LIM domain	lateral signaling for cell migration	immunoprecipitation	10	500−600aa (N-terminal region outside of PH domain)
ArhGAP23	Ankfy1	BTB, ankyrin repeat	Rab5 effector	affinity purification tag	41	N.D.

RhoGAP	predicted interactor	domain architecture	signaling pathway	methods	score (ELM)	predicted interacting region
ArhGAP21	Lyn	Tyr kinase, SH3, SH2	PI3kinase-Akt signaling	ELM;LIG_SH3_1,3	1.327e-3	^{193}RNIPEPP^{199}, ^{806}IDEPTSP^{812}, ^{1093}TQSPHSP^{1099}
ArhGAP21	Lck	Tyr kinase, SH3, SH2	integrin signaling	ELM:LIG_SH3_1,3	1.327e-3	^{193}RNIPEPP^{199}, ^{806}IDEPTSP^{812}, ^{1093}TQSPHSP^{1099}
ArhGAP21	Sorbs2	Tyr kinase, SH3, SH2	organization of postsynaptic complex, dendritic development	ELM:LIG_SH3_1,3	1.327e-3	^{193}RNIPEPP^{199}, ^{806}IDEPTSP^{812}, ^{1093}TQSPHSP^{1099}
ArhGAP21	casein kinase II	Ser/Thr kinase	dendritic spine formation, IS protein clustering	ELM:MOD_CK2, D_2P_2	1.457e-2	^{870}QPNSKTE^{876}, ^{877}RSKSYDE^{883}, ^{920}RKDSSSE^{926}
ArhGAP21	RhoB	RhoGTPase	synaptic plasticity, dendritic spine formation	docking by HDOCK		RhoGAP domain with C-terminal 22aa
ArhGAP21	RhoC	RhoGTPase	neuronal homeostasis, apoptosis	docking by HDOCK		RhoGAP domain with C-terminal 22aa
ArhGAP21	RhoG	RhoGTPase	actin-mediated transport, migration	docking by HDOCK		RhoGAP domain with C-terminal 22aa
ArhGAP21	Tc10	RhoGTPase	vesicular transport, neurite outgrowth	docking by Haddock		RhoGAP domain with C-terminal 22aa
ArhGAP23	PTEN	tensin phosphate, C2 domain	cell growth and apoptosis	docking by ACDP and MOE		PDZ domain (55−64aa)
ArhGAP23	Arf6	Arf domain	recruitment of endosomal coat complexes	docking by Haddock		ArfBD-like domain (688−836aa)
ArhGAP21	RhoD	RhoGTPase	Rab5-dependent endocytosis	docking by Haddock		RhoGAP domain with C-terminal 22aa
ArhGAP23				docking by HDOCK		RhoGAP domain
ArhGAP21	Cdc42	RhoGTPase	Golgi organization	docking by HDOCK		RhoGAP domain
ArhGAP23			cell motility	docking by HDOCK		RhoGAP domain
ArhGAP21,23	YWHAG	14-3-3	cytoskeletal reorganization	ELG:LIG_14-3-3, 14-3-3 binding motif	4.477e-3	^{473}RSASQGAL^{480}, ^{877}RSKSYD^{882}, ^{1075}RQSLS^{1079}(21), ^{620}RSKSCDDGL^{628} (23)
ArhGAP21,23	TNK2	Tyr kinase, SH3	receptor signaling	ELM:LIG_SH3_1,3	1.327e-3	^{193}RNIPEPP^{199}, ^{806}IDEPTSP^{812}, ^{1093}TQSPHSP^{1099} (21), ^{549}IDEPTSP^{555}, ^{581}GTSPSSP^{587}(23)
ArhGAP21,23	Arf3	Arf domain	recruitment of Golgi coat complexes	docking by Haddock		ArfBD (21), ArfBD-like domain (23)
ArhGAP21,23	RhoA	RhoGTPase	growth corn repulsion, regulation of neurite outgrowth and synaptic protrusion	docking by HDOCK		RhoGAP domain with C-terminal 22aa, RhoGAP domain (ArhGAP23)

[a]The putative domain or linear motifs predicted to mediate ArhGAP21/23 interaction were selected. It is assumed that the molecule is considered to be a putative interactor if the known binding protein is in the same class of protein family or presents a domain or motif known to interact with a predicted ArhGAP21/23 linear motif or their substrate including RhoGTPase or Arf-family protein.[57−59] [b]Yeast two-hybrid system. [c]MudPIT: multidimensional protein identification technology.

https://doi.org/10.1021/acsomega.2c08054
ACS Omega 2023, 8, 19249−19264

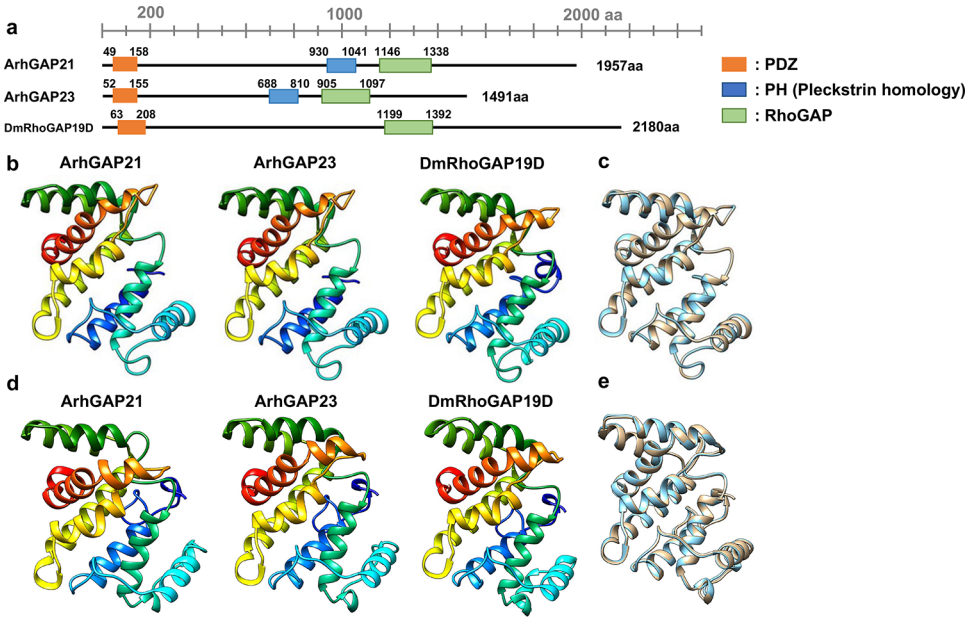

Figure 1. Modeled structure of the RhoGAP domains of ArhGAP21, ArhGAP23, and DmRhoGAP19D. (a) Schematic representation of ArhGAP21[8] and ArhGAP23 (orange box: PDZ domain, blue box: PH domain, green box: RhoGAP domain). UniProt and GenBank IDs are as follows: ArhGAP21: Q5T5U3-1/NM_20824.4; ArhGAP23: Q9P227-1/NM_001199417.2; and DmRhoGAP19D: Q9VRA6/NM_134552.6. (b) Modeled structure of the RhoGAP domain by homology modeling. RhoGAP domains are colored from the N-terminus (blue) to the C-terminus (red). (c) The modeled structure of the ArhGAP21 domain was superimposed over the RhoGAP domain of ArhGAP23. (d) Modeled structure of the RhoGAP domain generated by AlphaFold2.[21] (e) The modeled structure of the ArhGAP21 RhoGAP domain was superimposed over the RhoGAP domain of ArhGAP23. The modeled structure was evaluated by PROCHECK and ERRAT and visualized by the UCSF Chimera software program, version 1.15 (http://www.cgl.ucsf.edu/chimera).

similar folding structures (RMSD: 0.452 Å) (Figure 1e). Homology modeling and AlphaFold2 prediction showed similar ArhGAP21 and ArhGAP23 catalytic structures with RMSD values of 1.943 and 2.054 Å, respectively (Figure S3). Conformational differences in the loop region located between the 9th and 10th α-helices were detected in both the homology and AlphaFold-modeled RhoGAPs.

Both of the predicted RhoGAP models were subjected to molecular docking using the HDOCK software program, one of the most flexible prediction software programs for protein−protein interactions, to analyze the substrate availability for RhoGTPases.[33] Experimental PDB structures for the RhoGAP/RhoGTPase complex (PDB codes: 5irc, 1ow3, 1tx4, 3msx, 5c2j, 1grn, 2ngr) indicated that the catalytic arginine and +2 positions in the catalytic loop were close to glycine and alanine at the p-loop in the RhoGTPase family (Figure S4). The interaction details for the both the RhoGAPs were further investigated using the HADDOCK software program by setting the conditions for the mode of substrate recognition.[20,34,43] The predicted docking model was also checked by PRODIGY, which provides theoretical binding affinity of the complex[37] (Table 1). Several RhoGAPs analyzed for experimentally validated RhoGTPase affinities were selected as the modeled complex using HDOCK in template-free/hybrid mode.[44−46] As shown in Table S4, the binding affinities showed similar levels between the theoretical K_D value or binding free energy calculated by PRODIGY and corresponding parameters by isothermal titration calorimetry experiments or kinetic measurements, considering the species-specific diversities and experimental conditions for the substrate preferences (Table S4).

A computational analysis of alanine scanning mutagenesis by DrugScorePPI simulation was additionally performed to analyze their binding interface.[36] The property of interface residues was indicated by the degree of buriedness of each residue in the binding interface, where a high score is necessary but not sufficient for hot spot identification (Figure S5). The template-based model of the ArhGAP21 domain was predicted to interact well with Cdc42 (Figures 2a, 3a, and 4a), analogous to the MgcRacGAP-Cdc42 structure (PDB code: 5c2j), in both the HDOCK and HADDOCK software programs. The binding analysis by PRODIGY showed the predicted binding affinity (ΔG) and dissociation constant (K_D) to be −10.1 kcal/mol and 8.2×10^{-8} M (Table 1), respectively. The predicted interface of the RhoGAP structure in modeled ArhGAP21 was very similar to that of the MgcRacGAP-cdc42 complex (PDB code: 5c2j) (Figures S4 and S5a). In contrast, RhoA was not selected from the predicted ArhGAP21 structure by HDOCK in template-free mode, although the RhoGAP was deduced to interact with RhoA, with low affinity according to HADDOCK and PRODIGY (8.0×10^{-6} M). The ArhGAP23 structures selected by homology modeling and AlphaFold were also predicted to specifically interact with cdc42 or RhoA (Figure 3i,j and Figure S6). Cdc42 and RhoA complexes were retrieved by AlphaFold and homology-modeled structure with RMSD values of 0.389 and 0.246 Å, respectively, from all the docking models (Figures 2h,i, 3i,j, 4h,i and Figure S7d). These models interacting with cdc42 and RhoA showed respective binding affinities of −10.0 and −12.0 kcal/mol and dissociation constants of 9.6×10^{-8} and 3.3×10^{-9} M (Table 1). The binding energy calculation of ArhGAP23 to cdc42 and RhoA showed interfacial hotspots at the conserved residues near the catalytic arginine finger and hydrophilic interface (Figure S5a). Rac1 interaction with the RhoGAPs ArhGAP21 or ArhGAP23 was not detected by HADDOCK or HDOCK using the prediction method, although the RhoGAP N-chimerin

https://doi.org/10.1021/acsomega.2c08054
ACS Omega 2023, 8, 19249−19264

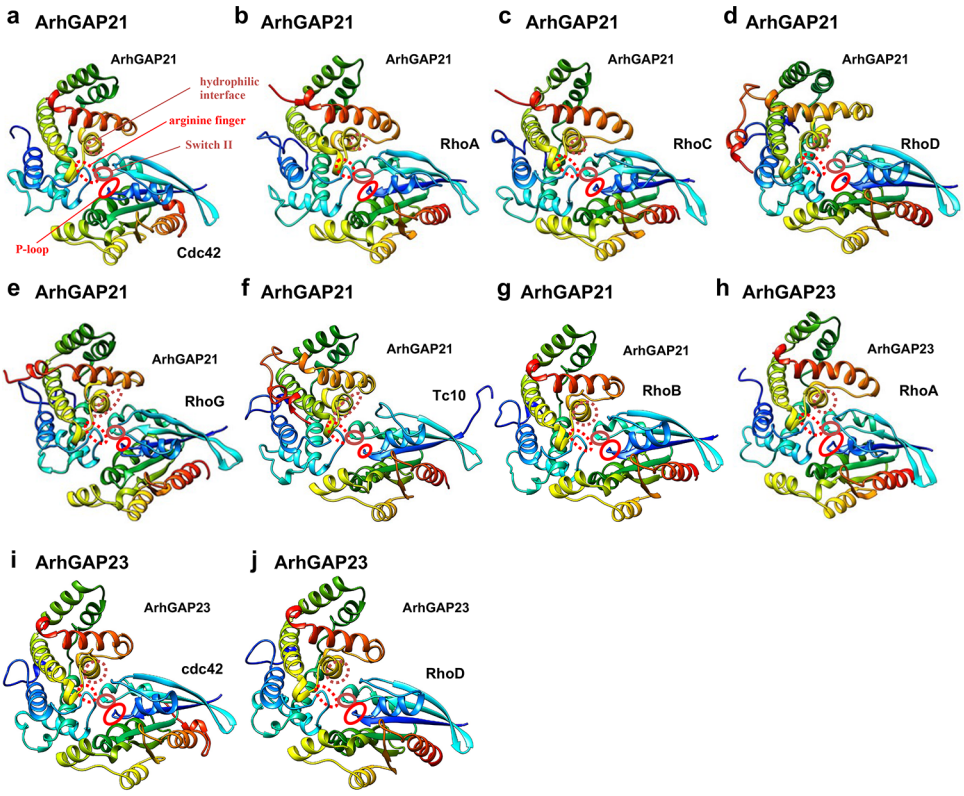

Figure 2. RhoGTPase recognition model generated by modeled ArhGAP21 and ArhGAP23. RhoGAP domains of homology-modeled ArhGAP21 (a–f) bound to Cdc42 (a), RhoA (b), RhoC (c), RhoD (d), RhoG (e), and Tc10 (f) and ArhGAP23 interacting with RhoA (h) were searched using the HDOCK and HADDOCK software programs, and the better structural model was selected for each docking model (a: HDOCK, template-free mode; b, c, e, h: HDOCK, hybrid mode; d, f: HADDOCK). AlphaFold-based modeled ArhGAP21 bound to RhoB (g) and ArhGAP23 bound to cdc42 (i) and RhoD (j) were also selected using the HDOCK and HADDOCK software program (g, i, j: HDOCK, template-free mode). Docking models were assessed by the proximity of the conserved region in the interface in RhoGAP to switch II and p-loop of RhoGTPase proteins. The RhoGAP substrates obtained by both software programs were structurally examined. Cdc42 and RhoA were fitted well to both ArhGAP21 (a, b) and ArhGAP23 (h, i). Conserved regions consisted of an arginine finger (red dotted circle) and hydrophilic interface (orange dotted oval) in RhoGAP domains facing to switch II (orange oval) and p-loop (red circle) of RhoGTPases (a–j).

deduced from 3cxl was theoretically selected as a Rac1 binding protein by HDOCK (Figure S1). The proximity of the catalytic arginine finger to the corresponding residues in the p-loop of the modeled 3cxl-Rac1 complex was also detected, as were RhoA/Cdc42-RhoGAP complexes (Figure S5b). The modeled ArhGAP21 bound to RhoC was also selected based on the AlphaFold-based prediction (Figure S7b).

To gain more insight into the substrate recognition mechanism, the ArhGAP21 domain, including the region outside of the 22 C-terminal residues, was modeled using trRosetta and AlphaFold2, and the output models were evaluated using PROCHECK and ERRAT for homology modeling. The model3 predicted by trRosetta was evaluated as the best according to the scores and template ArhGAP2 structure by homology-based prediction (Table S2). The selected model3 also showed high scores in structural quality according to the verify3D and PROSA software programs. The energy minimization process using the MOE system revealed that both the template-based model and predicted trRosetta model3 of the ArhGAP21 RhoGAP domain showed overall quality scores that were better than or the same as the ERRAT and PROCHECK energy minimized models, respectively. The predicted model3 showed a better score in Verify3D than the energy minimized structure model and *vice versa* for the template-based model.

After the selected model was applied to the docking procedures by the HDock and Haddock software programs, RhoA was fitted well to the RhoGAP domain in all software programs, indicating that the C-terminal flexible region outside of the RhoGAP domain determines the RhoA specificity of ArhGAP21 in the tertiary structure model (Figures 2b, 3b, and 4b; Table 1). The RhoGAP domain with the C-terminal region was structurally modeled using the AlphaFold software program. Homology and AlphaFold modeled structures showed regional differences in the loop region between the first and second α-helices and the fourth α-helix in the RhoGAP domains with an RMSD value of 1.33 Å except for the flexible 21C-terminal amino acids. In case of the AlphaFold predicted model, Cdc42 but not RhoA was selected as the substrate using the corresponding region of ArhGAP21, showing similar affinity to that with the homology-modeled RhoGAP model (K_D: 3.5×10^{-8} M) (Figure S7a). The critical interface residues of the RhoA complex located in the conserved interfaces and catalytic regions showed a similar pattern to the p50RhoGAP-RhoA complex (PDB code: 1tx4) (Figure 4b). The binding affinity was −11.3 kcal/mol, and the K_D value was 1.1×10^{-8} M (Table 1). When the predicted homology-modeled ArhGAP21 structures interacting with RhoA and Cdc42 were superimposed onto each other, both conformations were found to be different, especially in the loop region between the 3rd and 4th α-helices and the N-

https://doi.org/10.1021/acsomega.2c08054
ACS Omega 2023, 8, 19249−19264

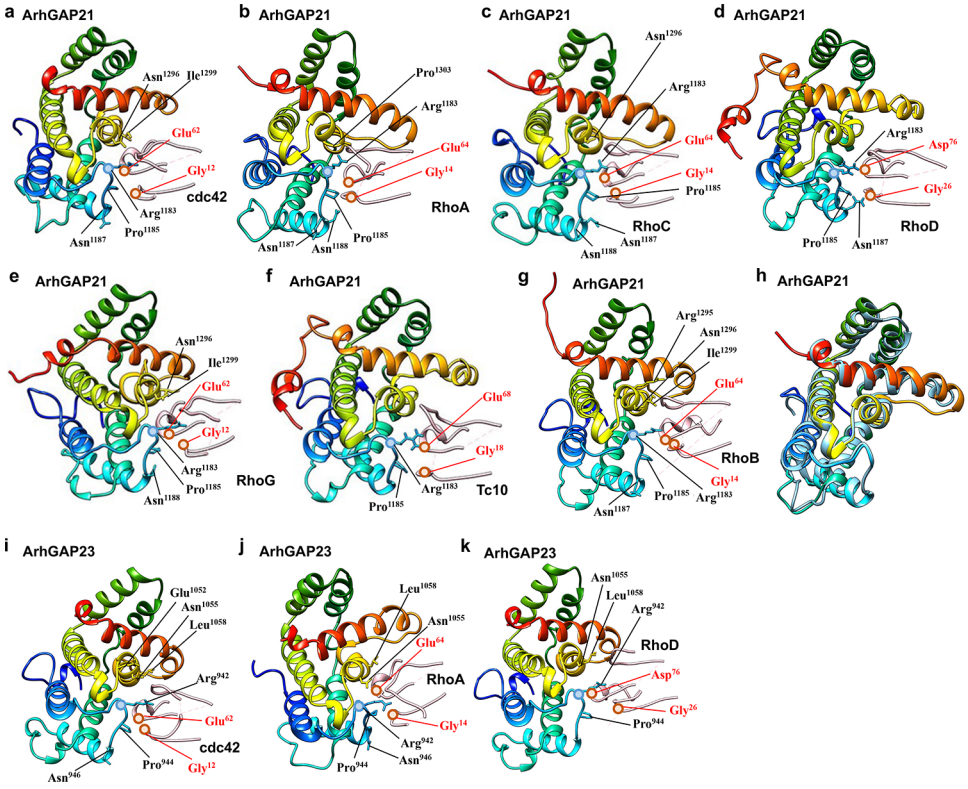

Figure 3. Interface model of ArhGAP21 and ArhGAP23 bound to conserved binding regions in RhoGTPases. The residues of RhoGAP structure involved in interaction with the p-loop and switch I/II in each RhoGTPase were examined, and the tertiary orientation of the side chains is indicated in the RhoGAP structure of ArhGAP21 (a–g) or ArhGAP23 (i–k). ArhGAP21-RhoGAP domains bound to RhoA (colored) and Cdc42 (light blue) were superimposed (h).

terminal 10th α-helix in the RhoA-bound form (Figure 3h). HDOCK docking analysis also selected the AlphaFold-modeled ArhGAP21 bound to Tc10 (Figure S7c). RhoB, RhoC, RhoG, and Tc10 displayed a good fit to the RhoGAP domain of ArhGAP21 with predicted hotspots in their conserved regions but not to the RhoGAP domain of ArhGAP23 (Figures 2c,e–g, 3c,e–g, and 4c,e–g; Figure S5a). RhoD was predicted to interact with the ArhGAP21 and ArhGAP23 domains using the homology modeling and AlphaFold, respectively (Figures 2d,j, 3d,k, and 4d,j). Predicted K_D values for the interaction with RhoD or Tc10 showed a lower affinity than that with other RhoGTPases, although their theoretical substrate recognition modes were fitted to the experimental K_D values obtained by RhoGAP reaction[47] (Table 1, Table S4). The interfacial hotspots were located in the conserved region around the catalytic arginine finger (Figure S5a). RhoGTPases possess variable residues in the N-terminal region of the third α-helix, and these residues were predicted to form the interface with the catalytic loop of the modeled RhoGAPs (Figure 4a–j). The variable Asp^{90} residue in the RhoA and the Asn^{92} residue in the Cdc42 interfaces plays a critical role in their interactions with ArhGAP21 or ArhGAP23, as indicated in the binding free energy calculation (Figure 4a,b,h,i; Figure S5a). The conserved Asp residue in the switch II region of RhoGTPases also plays a critical role in the interactions with both RhoGAPs (Figure 4, Figure S5a).

RhoGAP19D, the *Drosophila* ortholog of ArhGAP21, was also predicted by the HHPred search, and potential templates generated by trRosetta and I-Tasser were also selected for ArhGAP2 (PDB code: 3cxl) and glucocorticoid receptor DNA binding factor1 (PDB code: 3fk2) (Figure 1b, Table S1). An evaluation by PROCHECK and ERRAT selected ArhGAP2 as the best template for *Drosophila* RhoGAP19D (Table S2). The best predicted model was ArhGAP2, with a QMean score of 0.77, and the multiple sequence alignment of its RhoGAP domain showed 44.6 and 42.1% sequence homology with human ArhGAP21 and ArhGAP23, respectively (Figure 1b, Figure S2c). The AlphaFold-based model showed a similar structure to the homology-modeled structure (Figure 1d).

Substrate selection by the homology modeled and AlphaFold-based structural prediction based on PRODIGY analysis deduced the ArhGAP21 or ArhGAP23 preference to Cdc42, RhoA, RhoB, RhoC, and RhoG (Table 1) or Cdc42 and RhoA, respectively, from the structural aspects. Although Rac1 was shown to be the RhoGAP substrate in previous reports,[16,42] neither of the modeling methods selected the RhoGTPase, suggesting that a conformational change in RhoGAP might be involved in the recognition processes. RhoA and RhoC activities are modulated by ArhGAP21 silencing and knockout conditions in a cell-type-specific manner, and our prediction results are consistent with the previous findings.[9,11,48]

Type I and III Arf Proteins Are Predicted to Interact with ArhGAP21 and ArhGAP23. The PH domains are sequentially conserved among vertebrate ArhGAP21/23 proteins, whereas RhoGAP19D does not possess its signature (Figure 1a). ArhGAP21 is known to associate with Arf1 and Arf6 via the ArfBD, which includes the PH domain and is located at the N-terminus of the RhoGAP domain.[7,49] This association is mediated by the loop region of $\beta 5'$-$\beta 6'$ sheets and the C-terminal α-helix of ArhGAP21 located between switch I and the interswitch region of the GTP-bound form of Arf in the

https://doi.org/10.1021/acsomega.2c08054
ACS Omega 2023, 8, 19249−19264

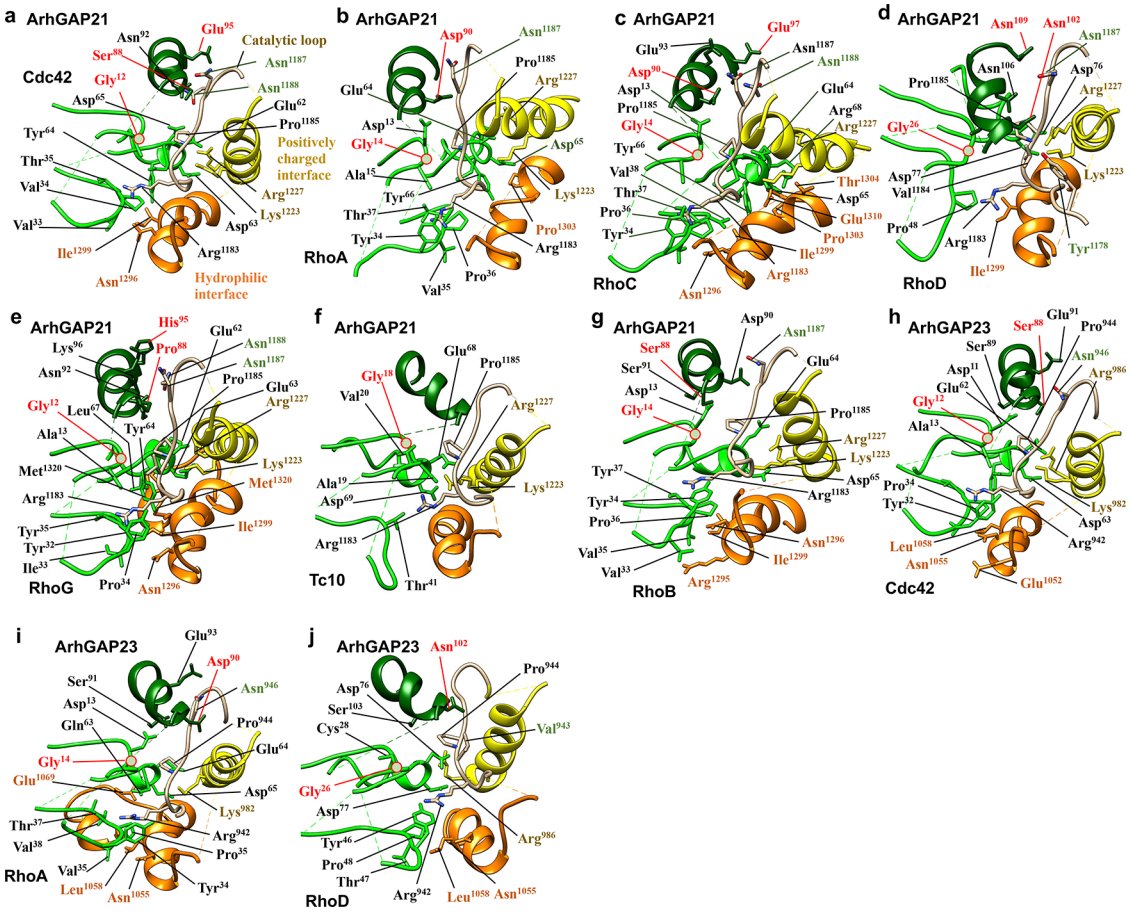

Figure 4. Deduced catalytic residues in ArhGAP21 and ArhGAP23-RhoGTPase complexes. The conserved p-loop−switch I/II region of RhoGTPases (green) and variable residues located at the interface of RhoGTPase (marked with red letters in dark green ribbon) were predicted to form the RhoGAP catalytic interface (a−j). Side chains of the arginine finger in the catalytic loop (gold), the conserved positively charged interface (yellow), and conserved residues in the hydrophilic interface (orange) of RhoGAP are indicated in the modeled catalytic interfaces of ArhGAP21 (a−g) and ArhGAP23 (h−j). The interfacial residues of the RhoGAP domain for selective Rho-, Cdc42-, or Rac-selective interaction are indicated (green letters). The modeled structure was evaluated by DrugScorePPI, and side chains of the selected catalytic interface were visualized using the UCSF Chimera software program, version 1.15.

complex.[7] The ArfBD of ArhGAP21 (PDB code: 2j59) was examined to determine which Arf proteins could interact using HDOCK and HADDOCK by setting the constraints according to the crystallographic structure of the complex. Arf3 (PDB code: 6ii6) and Arf6 (PDB code: 2j5x) were selected based on the interaction within the corresponding region by HADDOCK, and the HDOCK results in template-free mode supported this prediction (Figure 5b,c). The interfacial hotspots were located in the $\beta 5'$-$\beta 6'$ sheets for Arf3 interaction, and the theoretical binding affinity was −8.4 kcal/mol (K_D: 1.3 × 10^{-6} M) (Figure S5c, Table 1).

The ArfBD of ArhGAP23 showed 47.2% sequence homology with the corresponding matched region of ArhGAP21 in MAFFT alignment, and structural modeling of ArhGAP23 was performed using the HHPred software program. The modeled ArhGAP23 structure predicted Tiam1 (PDB: 4k2p) and ArhGAP21 (PDB code: 2j59) as candidate templates (Table S1, Figure 5a). The best model, based on the ArhGAP21 template, was selected by evaluating the structural quality check using PROCHECK and ERRAT (Figure 5a, Table S2). The QMean score of 0.70 showed a high reliability for this model (Table S1, Figure S8a). The modeled domain structure was examined for interactions with Arf-family proteins using the HADDOCK and HDOCK software programs. The docking test selected Arf1, Arf3 (PDB code: 6ii6), and Arf6 (PDB code: 2j5x), with RMSD values of 0.372, 0.498, and 0.729 Å, respectively, as the structural fitted model (Figure 5d−f). The critical conserved residues of the Arf-binding region in ArfGAP23 showed identical patterns to those of ArfGAP21, except for Leu^{826} corresponding to Ile^{1057} of ArhGAP21 in the C-terminal α-helix (Figure S5c). The interfacial hotspots of ArhGAP23 for Arf3 binding were similarly located in the $\beta 5'$-$\beta 6'$ sheets as with the case of ArhGAP21-Arf3 interaction (Figure S5c). Type II Arf-family proteins such as Arf4 (PDB code: 1z6x) and Arf5 (PDB code: 2b6h) were not selected as ArhGAP21 or ArhGAP23 Arf-binding regions using either HDOCK with template-free mode or HADDOCK. The ArfBD of ArhGAP23 was also modeled by the AlphaFold2 software program (Figure S8b), and the docking test selected Arf3 as the complex with the ArhGAP23 domain using both docking software programs (Figure S9). Arf1 (2j59), Arf4 (1z6x), and Arf6 (2j5x) were predicted as the complex of the corresponding ArfGAP23 region by the HADDOCK software program, but none of the Arf proteins was selected using the HDOCK software program in template-free mode (data not shown). Although the Tyr^{767} and Ile^{822} residues in binding free energy in the homology-modeled ArhGAP23 bound to Arf3 showed relatively lower

https://doi.org/10.1021/acsomega.2c08054
ACS Omega 2023, 8, 19249−19264

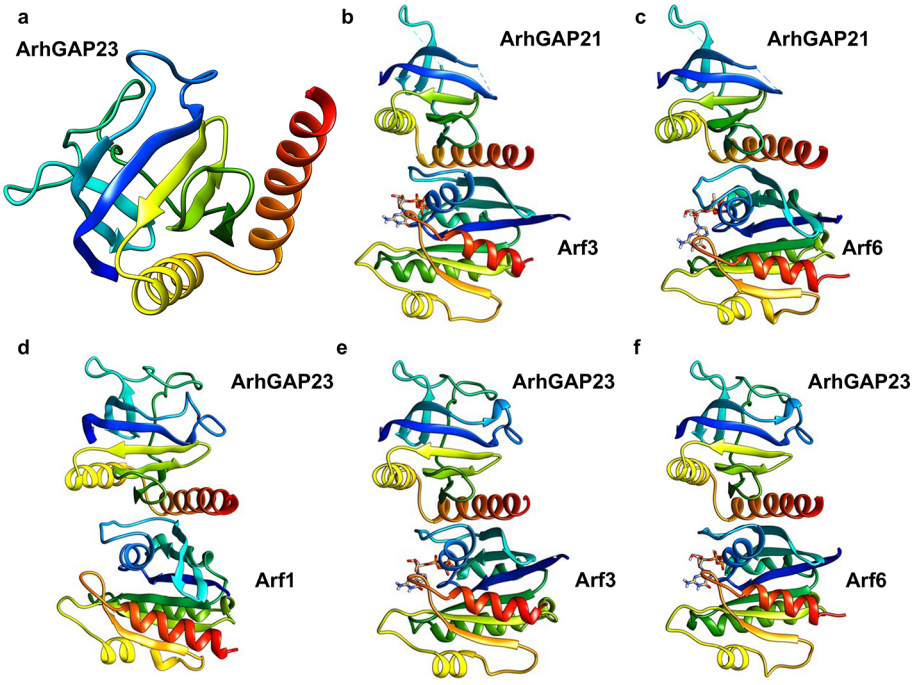

Figure 5. Interaction of ArhGAP21/23 with Arf-family proteins. Modeled structure of the Arf binding region of ArhGAP23 containing the Pleckstrin homology domain (a). Predicted ArhGAP21-Arf3 complex (b) and ArhGAP21-Arf6 (c) complexes calculated from PDB (PDB code: 2j59[7]) are shown as colored ribbons from the N-terminus (blue) to the C-terminus (red). Homology-modeled ArhGAP23-Arf1 (d), ArhGAP23-Arf3 (e), and ArhGAP23-Arf6 (f) complexes were predicted based on the selected tertiary structure (a). The GTP-bound form of Arf1 (PDB code: 2j59) or Arf3 (PDB code: 6ii6) or GTPγS-bound form of Arf6 (PDB code: 2j5x) was used for docking tests with the HADDOCK and HDOCK software programs. Each complex is indicated as a ribbon from the N-terminus (blue) to the C-terminus (red). Modeled structures were evaluated by DrugScorePPI and visualized by the UCSF Chimera software program, version 1.15.

values than the Arf1 complexes, the conserved residues in the interface of the predicted complex were preserved in AlphaFold-based docking models (Figure S9), suggesting that subtle conformational changes in the interface may be required for the optimal recognition of Arf3 protein.

Homology modeling predicted RhoGAP and ArfBD structures accurately because all of the identities between a target sequence and the template structures were more than 30% (Table S1). The threading method using I-Tasser[24] can be used for the sequences showing an extremely low identity to templates, and multiple scoring systems for a target sequence and multiple structural templates from the Protein Data Bank can help improve the modeling accuracy. Structure prediction and modeling using trRosetta,[25] which applies inter-residue geometry from multiple sequence alignments with restraints of distance and orientation, provided more accurate models for the substrate interaction test than the Robetta program that utilizes a combination of template-based modeling with fragment-based and contact-assisted folding. Structural evaluations using PROCHECK, Verify3D, and ERRAT selected the most appropriate models. In addition, regarding RhoGAP prediction models, structural prediction using AlphaFold2 selected RhoB and RhoD as the predicted substrates of ArhGAP21 and ArhGAP23, respectively, agents that were not chosen by the docking analysis for homology modeling (Figures 2−4). Regarding the ArhGAP23 PH domain, the homology modeled structure for Arf interactions was consistent in the specificity obtained by the HDOCK and HADDOCK docking software programs, but an HDOCK analysis using an AlphaFold-based structural model did not match the experimental results reported previously.[8]

PDZ Regions of ArhGAP21/23 Possess a Conserved Globular Structure with Analogy to the MAST-Family PDZ Domains, and PTEN-ArhGAP23 PDZ Interaction Was Structurally Modeled. Structural prediction of the PDZ domain of ArhGAP23 selected MAST2 (PDB code: 2kyl) and ArhGAP21 (PDB code: 2yuy) as the templates with QMean scores of 0.49 and 0.82, respectively, using SWISS-MODEL (Figure 6a). The evaluation of these structural models by ERRAT and PROCHECK identified the ArhGAP21 PDZ domain as having better scores than the MAST2 PDZ domain (Figure 6b, Table S2). The corresponding region of the PDZ domain was also structurally modeled by the AlphaFold software program (Figure S10a). The predicted model showed similar folding to the template-based PDZ domain model, except in the loop region, with an RMSD value of 2.11 Å in the structurally conserved N- (Asp^{52}-Phe^{61}) and C-terminal (Val^{100}-Lys^{154}) regions (Figure S10b). To characterize the PDZ sequence in ArhGAP21/23, a PSI-BLAST search in the GenBank database was performed for both domains as query sequences, and PDZ domains of MAST family proteins were selected based on the top-ranked scores (Figure 6c). The MAST-family PDZ domains contain globular folding structures similar to the ArhGAP21/23 PDZ domains (PDB codes, MAST1: 3ps4, MAST2: 2kyl, MAST3: 3khf, MAST4: 2w7r[50]), except for the loop region connecting the conserved regions (Figure 6c−e, Figure S11). The ArhGAP21/23 PDZ domains contain the FTLRXXXVY sequence conserved with the MAST2-PDZ domain that mediates interaction with the PTEN C-terminal region (PDB code: 2kyl). Whereas PTEN has been reported as a regulator of the β-arrestin1/ArhGAP21 complex in carcinoma, the resultant model implied the complex PTEN regulation upon Cdc42

https://doi.org/10.1021/acsomega.2c08054
ACS Omega 2023, 8, 19249−19264

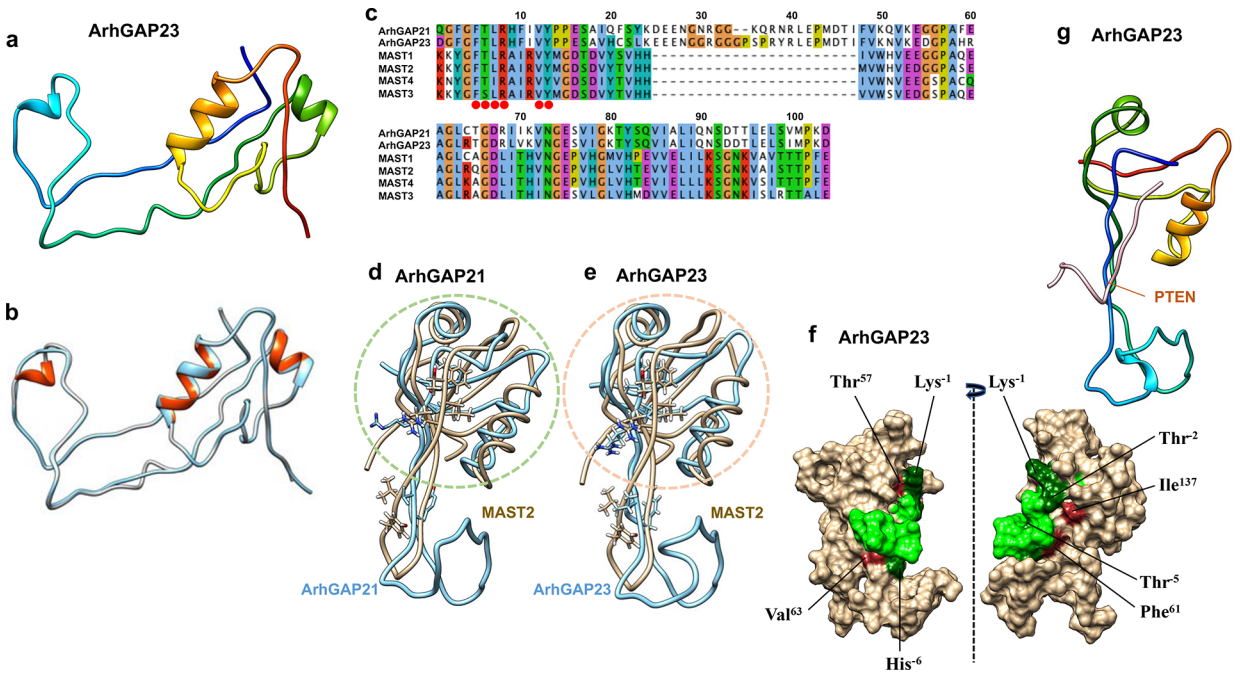

Figure 6. Conserved globular structure of ArhGAP21/23 PDZ domain with MAST proteins. (a) Modeled structure of the ArhGAP23 PDZ domain. Structural models were predicted by homology modeling with SWISS-MODEL. (b) The predicted ArhGAP23 PDZ structure (red: α-helices: gray; loops) was superimposed over the ArhGAP21PDZ domain (blue, PDB code: 2yuy). (c) Multiple sequence alignment of PDZ domains of ArhGAP21, ArhGAP23, and MAST-family proteins using the MAFFT software program.[32] Each PDZ domain structure of ArhGAP21 (d) or ArhGAP23 (e) modeled using SWISS-MODEL[23] was superimposed over the MAST2 PDZ domain, which interacts with the PTEN C-terminal tail (PDB code: 2kyl). The Phe, Ser, Leu Arg, Val, and Tyr residues of side chains in the PDZ domains of ArhGAP21 and ArhGAP23 conserved among MAST2-PTEN binding interface showed similar orientations (d and e) and are indicated as red circles in the sequence alignment (c). The N- and C-terminal parts of ArhGAP21 and ArhGAP23 form a globular domain similar to MAST-family proteins (2kyl, 3ps4, 3khf, and 2w7r;[50] Figure S11) and indicated as circles with dotted lines. (f) The modeled PDZ structure of ArhGAP23 (gold) was predicted to interact with the 13-mer PTEN peptide[89] (green) that tethers to the groove formed by the conserved region in the PDZ domain according to template docking using the MOE system. Predicted critical residues for the interaction of the ArhGAP23 PDZ domain (brown) and PTEN peptide (dark green) are indicated based on analogy with the PTEN-bound MAST2 tertiary structure[89] (PDB code: 2kyl). (g) Predicted ArhGAP23-PDZ interaction with the PTEN C-terminal peptide was determined by template docking using the MOE system. The structure of ArhGAP23 PDZ is colored from the N-terminus (blue) to the C-terminus (red) by UCSF Chimera (pink: PTEN peptide: PFDEDQHTQITKV). The modeled structure was evaluated by DrugScorePPI[36] and visualized using the UCSF Chimera software program, version 1.15.

activation by β-arrestin1 and ArhGAP21.[51] Although β-arrestin1 is known to bind to the RhoGAP C-terminal region, ArhGAP21 was not included as a stable β-arrestin1 complex in the proteomic analysis.[9,52]

To clarify this contradiction, the interaction of PTEN to the ArhGAP21/23 PDZ domain was predicted by template docking using the MOE system. ArhGAP-PDZ domains were examined by template docking using the known structure of the PTEN 13-mer peptide (PDB code: 2kyl). MAST2-PDZ has a class I domain-specific motif that recognizes the consensus sequence Ser/Thr-*X*-Φ (*X*: any residue, Φ: hydrophobic residue).[53] The ArhGAP21 PDZ domain was similarly structured but did not completely correspond to MAST2-PDZ in several aspects. In contrast, ArhGAP23 was predicted to possess the same interaction network as the MAST2-PTEN complex (Figure 6f). The ArhGAP23 PDZ backbone amides of Phe^{54}, Gly^{55}, and Phe^{56} that were hydrogen-bonded to the C-terminus of the PTEN peptide were partially conserved with the MAST2-PDZ domain, whereas PTEN Lys$^{(-1)}$ was predicted to interact with the side chain of its Thr^{57} in PDZ through hydrophobic association (Figure 6c,f). Simulation using DrugScorePPI predicted that hot spots in the ArhGAP23 PDZ domain were localized at Asp^{52}-Val^{63} and Ile^{140}-Leu^{147}, including the conserved region (Asp^{1}-Val^{12} and Ile^{89}-Leu^{96} in Figure S5d). The side chain of Thr$^{(-2)}$ in the PTEN peptide was predicted to form a hydrophobic interaction with the side chain of the conserved Ile^{137} in the α-helix of ArhGAP23 PDZ, analogous to Val^{77} in MAST2-PDZ. Ile$^{(-3)}$ is stabilized by hydrophobic contact with the side chain of Arg^{22} in the MAST2 β-sheet. Nevertheless, this mechanism was not predicted to be structurally conserved in the case of ArhGAP23 PDZ, although Arg^{59} in ArhGAP23 PDZ is located in the same position as MAST2.[53] His$^{(-6)}$ and Thr$^{(-5)}$ of PTEN were located in close proximity to the conserved side chains of Val^{63} and Phe^{61} in the ArhGAP23 PDZ domain, respectively, in an orientation similar to that of the MAST2-PTEN complex (Figure 6g). The binding affinity (ΔG) calculated by a PRODIGY analysis was −7.3 kcal/mol, and the dissociation constant was estimated to be 6.8×10^{-6} M at 37 °C (Table 1). A majority of Arf6 GEFs or GAPs are activated in the presence of PIP_2.[54] PTEN may be involved in the Arf regulation coupled with RhoGTPase downregulation. PI3-kinase regulates filopodia formation through actin bundles with cdc42 activation and dendritic spinogenesis. PTEN-ArhGAP23 signaling may also be important for the regulation of F-actin patches.[55,56]

Neuronal ArhGAP21/23 Interaction Networks. Although ArhGAP21 and ArhGAP23 are co-expressed in many regions of the developing brain in humans, their neuron-specific functions remain poorly unexplored.[41] Domain signatures for

https://doi.org/10.1021/acsomega.2c08054
ACS Omega 2023, 8, 19249−19264

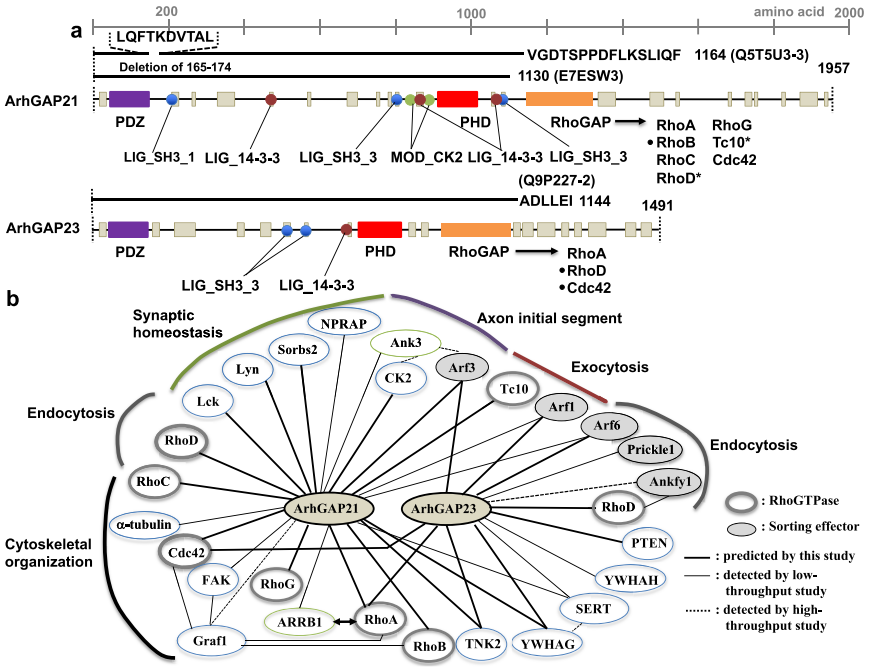

Figure 7. Neuronal ArhGAP21/23 interaction networks. (a) Interaction mapping of putative ArhGAP21 and ArhGAP23 interactors. Both the ArhGAP21 and ArhGAP23 proteins are represented by a disordered domain (gray), PDZ (purple), PH (red), and RhoGAP (orange) domain with sequence boundaries of the human RhoGAPs (ArhGAP21: Q5T5U3, ArhGAP23: Q9P227-1). The indicated domains were retrieved from the InterPro search,[30] and the interaction signatures were deduced based on the conserved linear motif.[57−59] Canonical LIR motifs required for the SH3-containing proteins (LIG_SH3_1 and 3) (light blue circle), 14-3-3 binding site (LIG_14-3-3) (brown circle), and CK2 phosphorylation site (MOD_CK2) (green circle). Alternative ArhGAP21 and ArhGAP23 isoforms are indicated. The ArhGAP21 isoform (UniProt ID: E7ESW5-1, 1130 residues) is missing a C-terminal region (827 residues). The C-terminus of another isoform (UniProt ID: Q5T5U3-2, 1164 residues) was truncated at residue 1158 and substituted with VGDTSPPDFLKSLIQF. This isoform also lacks ^{165}LQFTKDVTAL^{174}. The short ArhGAP23 isoform (UniProt ID: Q9P227-2) is truncated at residue 1138 with substitution in the region from positions 1139 to 1144 (ADLLEI). (b) ArhGAP21 and ArhGAP23 interactors identified by low-throughput data (thin line),[7−10,17,63,67,72,82−84] selected by structural modeling and the prediction based on a linear motif (bold line),[66,68,69] and predicted by high-throughput interaction data (dotted line).[67,78,84] The asterisk in RhoGTPase shown in panel a indicates RhoGAP substrates selected by HADDOCK but not HDOCK template-free mode. The dot symbol (•) indicates the predicted interactor based on the structural modeling by AlphaFold[21] using the HDOCK software program. Arf proteins or the primary sorting interactors regulating intracellular transport (shaded oval) and RhoGTPase (bold-line oval) are shown to categorize the interactions by the intracellular signaling.

putative interactors regulating neuronal signaling were analyzed based on deduced ArhGAP21 and ArhGAP23 localization in view of the predicted Arf binding properties and high-throughput association studies, including BioGrid and IntAct[39,40] (Table S5). Evolutionarily conserved disordered domains, a particular stretch of amino acid patterns, or conserved regions with predicted linear motifs were also considered in the prediction for the interactors (Figure 7a).[57−59] Because disordered regions can be modified by phosphorylation or provide an interface to specific binding partners for signaling, ArhGAP21/23 binding proteins were additionally examined by curating the relevant literature (Table 2). These findings were used to expand the assembly of the ArhGAP21 and ArhGAP23 interaction networks considering their intracellular localization and RhoGAP substrates (Table 2, Figure 7b). A putative interaction motif was selected based on its location within the disordered domain mapped by ELM,[60] D_2P_2,[61] and MobiDB,[62] and casein kinase (CK) phosphorylation sites were predicted by the disordered propensity and phosphosite because CK regulates neuronal cytoskeletal dynamics and subcellular membrane targeting. Motif conservation through mammalian ArhGAP21/23 orthologs was also considered to select the functional interaction sites.

High-throughput proteomic studies of ArhGAP21 and ArhGAP23 binding proteins include interphase and mitotic regulators presumably bound to 14-3-3 proteins that function in nuclear transport or transcription.[63] 14-3-3η and 14-3-3σ were selected as ArhGAP21 and ArhGAP23 binding proteins, respectively, and 14-3-3γ was additionally predicted for interacting with ArhGAP21 and ArhGAP23 (LIG_14-3-3)[64,65] (Figure 7a, Table 2). Both RhoGAPs contain canonical Arg-containing phosphoserine motifs adjacent to the PH domain and an N-terminal disordered domain.[66] Interestingly, both ArhGAP21 and ArhGAP23 activities are also involved in serotonin transporter-dependent signaling.[17] ArhGAPs-14-3-3γ association was predicted in the SERT interactome (Figure 7b). Functional regulation of 14-3-3γ or suppressed RhoGTPase signaling in pathfinding may be required for neuronal migration and wiring during neurodevelopmental processes.

ArhGAP21 and ArhGAP23 were predicted to mediate the interaction with Arf1 and Arf6 through the PH domain, and their multiple effectors were shown to be localized in secretory and endocytic pathways. Therefore, the analysis of their interactors was also mainly focused on Arf- and RhoGTPase-regulated signaling. Neuronal ArhGAP21 and Ank3 were localized in the axonal initial segment (AIS) region, and Ank3 was selected as the ArhGAP21 complex from the BioGrid

https://doi.org/10.1021/acsomega.2c08054
ACS Omega 2023, 8, 19249−19264

database[15,67] (Table 2, Figure 7b). CK2 potentiates the clustering localization of Nav1.2 to the AIS through phosphorylation in the ankyrin binding repeat.[68] ArhGAP21 contains three potential CK2-mediated phosphorylation sites (MOD_CK2) in the N-terminus of its PH domain, but no potential CK2 phosphorylation site was selected in ArhGAP23. PSI-Pred predicted a coiled structure including the CK2-phosphorylated region in ArhGAP21 (851−930 residues), similar to the corresponding sites within the ankyrin-binding motif of Nav1.2.[69] Arf3 was predicted to interact with ArhGAP21 and was enriched at the AIS. Pathogenic variants of Arf3 have been reported to cause ID.[70,71] Arf3 binding and CK2 regulation by ArhGAP21 may target and maintain the RhoGAP activity in AIS during neuronal maturation. Whereas ARRB1 was identified as an ArhGAP21 binding protein,[9] the same C-terminal region outside the RhoGAP domain prerequisite to the ArhGAP21 interaction determined the specificity of its RhoGAP toward RhoA (Table 2; Figures 2b, 3b, 4b, and 7b). As the synaptic scaffold signaling, NPRAP, a brain-enriched p120 family protein, was identified in the ArhGAP21 complex.[72] The interactome for ArhGAP21-related signaling from the BioGrid database identified several proteins in the catenin family with the armadillo-repeats, including δ- and β-catenins, as a part of the ArhGAP21 complex.[41] NPRAP regulates dendritic and spine morphogenesis, and ArhGAP21 may specifically regulate RhoA signaling with p190RhoGEF.[73] Searching for ArhGAP21-interacting protein through its SH3 binding domain (LIG_SH3) in the disordered region led to the selection of Lck and Lyn (Table 2; Figure 7a,b). Tyrosine kinase nonreceptor2 (Tnk2) was also identified as an ArhGAP21 and ArhGAP23 interactor (Table 2). Tnk2 is enriched in the brain and contains an SH3 domain that binds to the proline-rich motif.[74] Both ArhGAP21 and ArhGAP23 may spatiotemporally regulate the synaptic homeostasis and cytoskeletal dynamics by interacting with Tnk2 during brain development.[18,75] Sorbs2 was identified as an ArhGAP21-specific interactor containing the PXXP motif, and their complex may regulate the core synaptic scaffolding network because the C-terminal SH3 domain of Sorbs2 mediates the binding to the postsynaptic protein SAPAPs (Table 2).[76]

In synaptic homeostasis, ArhGAP21 functions as an FMRP-targeting gene that is linked to mGluR signaling, as suggested by MeCP2 knockout mouse models treated with an mGluR5-negative allosteric modulator.[77] Treatment of cultured hippocampal neurons with DHPG, an mGluRI agonist, induces ArhGAP21 phosphorylation as a downstream cascade.[14] An *in vivo* embryonic brain interactome analysis revealed the presence of PSD scaffold proteins, such as several RhoGAPs and FMR interacting protein, which supports the physiological and pathological involvement of ArhGAP21 in developmental brain disorders.[18]

Prickle1 was identified as an ArhGAP23 binding protein for lateral signaling in migration[10] (Table 2, Figure 7b). RhoD is localized to Rab5-positive early endosomes by negatively regulating Rab5-mediated homotypic fusion, and ArhGAP21 and ArhGAP23 were predicted to regulate the RhoD activity, suggesting the role of RhoD in endocytosis in neurons[78] (Figure 7b, Table 2). Ankfy1 is a RhoD binding protein involved in the early endocytic pathway and was selected as interacting with ArhGAP23 based on the BioGrid database (Figure 7b), although RhoD recruitment to Ankfy1 depends on its isoprenylation and not its GTP-loaded status. ArhGAP21 is known to interact with Arf6, which is involved in the endosomal membrane recycling,[8,18,79,80] and ArhGAP21 and ArhGAP23 might play roles in the endosomal Prickle function in cooperation with RhoD activity in neurons.[10] RhoD is also known to interact with the actin nucleation factor WHAMM at the Golgi apparatus and regulate cell migration through actin reorganization.[81]

Regarding cytoskeletal regulation by ArhGAPs, α-tubulin regulates ArhGAP21 localization and functions[82] (Table 2, Figure 7b). Focal adhesion kinase (FAK) is an ArhGAP21 and Graf1 binding protein, and RhoA and Cdc42 may be cooperatively regulated by these RhoGAPs in dendritic organization[6,20,83,84] (Figure 7b). RhoB-knockout pyramidal neurons show complex dendritic blanching and immature spine development.[85] RhoB is transiently associated with active Src in the endosome for transport to the plasma membrane, and ArhGAP21 may be also involved in the downregulation of RhoB activity.[86] Tc10, which is closely related to cdc42-related RhoGTPase, as a postulated substrate of ArhGAP21, mediates exocytosis with its effector Exo70 and is downregulated at the plasma membrane.[87] It is required for the formation of neuronal polarity, and the exocyst complex is essential for membrane expansion in growth cones. ArhGAP21 may regulate neuronal exocytosis through Tc10 during the developmental neuronal wiring process. RhoG plays a critical role in actin dynamics, and ArhGAP21 may be involved in this process by targeting the small GTPases (Figures 2e and 7). Anillin is listed as a part of the ArhGAP21 complex in BioGrid, and its neuronal guidance co-effector RhoG was selected as the ArhGAP21 substrate;[88] however, the details of the physiological inhibition mechanism underlying the RhoG activity in the mammalian neuronal system remain largely unclear.[38] The present study sheds light on functional folding units by focusing on structurally validated effectors of ArhGAP21/23 RhoGAPs and will aid in the interpretation of the complicated pathological process of newly discovered ArhGAP21/23 gene variants.

CONCLUSIONS

Human ArhGAP21/23 RhoGAP domains were structurally modeled by the homology modeling method and the AlphaFold software program for rationalizing substrate recognition mechanisms, and the docking studies indicated the existence of multiple RhoGTPase substrates for each RhoGAP protein. Tertiary structural modeling of these RhoGAPs resulted in several intriguing findings: First, the conserved ArhGAP21 domain was predicted to recognize Cdc42, whereas the catalytic RhoGAP fold, including the outside region of the 22 C-terminal residues, was deduced to specifically catalyze RhoA, RhoB, RhoC, RhoD, RhoG, and Tc10. As ArhGAP23 substrates, Cdc42, RhoA, and RhoD were selected. Second, both the modeled ArfBD of ArhGAP23 and the corresponding region of ArhGAP21 interacted well with Arf1, Arf3, and Arf6 despite their sequence homology being lower than that of the other folding domains. Third, the predicted ArhGAP23 PDZ domain contained globular folding similar to that of the MAST-family PDZ domains and possessed the same conserved PTEN interaction network with the MAST2-PTEN complex. A binding analysis of the selected PDZ domain with disordered PTEN C-terminal peptides revealed that the conserved ^{57}TLRHF^{61} region in the PDZ domain with MAST-family proteins played a critical role as the binding interface with the PTEN C-terminus. Fourth, the interaction analysis predicted the physiological RhoGAP

https://doi.org/10.1021/acsomega.2c08054
ACS Omega 2023, 8, 19249−19264

functions of the ArhGAP21/23 as specific signaling hubs in intracellular transport, synaptic homeostasis, and cytoskeletal dynamics during neuronal development.

■ ASSOCIATED CONTENT

Supporting Information

The Supporting Information is available free of charge at https://pubs.acs.org/doi/10.1021/acsomega.2c08054.

Modeled structure of N-chimerin RhoGAP bound to Rac1 (Figure S1) and binding free energy calculation of the modeled complex (Figure S5b); superposition of RhoGAP domains of ArhGAP21, ArhGAP23, or *Drosophila* RhoGAP19D to each template structure (Figure S2); superposition of ArhGAP21 and ArhGAP23 RhoGAP domains predicted by homology modeling and AlphaFold2 (Figure S3); interaction matrix of the p-loop of RhoGTPases and catalytic residues of RhoGTPs (Figure S4); *in silico* alanine scanning of RhoGAP-RhoGTPase (Figure S5a), Arf binding region-Arf protein (Figure S5c), and ArhGAP23-PTEN interactions (Figure S5d); modeled structure of homology-modeled ArhGAP23 RhoGAP domain bound to Cdc42 (Figure S6) and AlphaFold-modeled RhoGAP domains of ArhGAP21 and ArhGAP23 interacting with RhoGTPases (Figure S7); superposition of modeled Arf binding domains of ArhGAP23 to the crystalized ArhGAP21 structure (Figure S8); AlphaFold-modeled Arf binding domain of ArhGAP23 bound to Arf3 protein (Figure S9); structure of PDZ domain of AlphaFold-modeled PDZ domain of ArhGAP23 and its superposition to homology-modeled PDZ structure (Figure S10); structural similarity of globular domains of ArhGAP21, ArhGAP23, and MAST-family proteins (Figure S11); HHPred template search summary of RhoGAP and Arf binding domains (Table S1); structural evaluation of the predicted domains of ArhGAP21 and ArhGAP23 (Table S2); tool information used for *in silico* analysis of ArhGAP21 and ArhGAP23 proteins (Table S3); binding affinities of RhoGTPases to RhoGAPs (Table S4); and information for accession code of RhoGAPs and their interactors (Table S5) (PDF)

■ AUTHOR INFORMATION

Corresponding Author

Zen Kouchi − *Department of Genetics, Institute for Developmental Research, Aichi Developmental Disability Center, Kasugai 480-0392 Aichi, Japan;* orcid.org/0000-0002-9138-3187; Email: zkouchi@inst-hsc.jp

Author

Masaki Kojima − *Laboratory of Bioinformatics, School of Life Sciences, Tokyo University of Pharmacy and Life Sciences, Hachioji 192-0392, Japan*

Complete contact information is available at: https://pubs.acs.org/10.1021/acsomega.2c08054

Author Contributions

Z.K. performed structural modeling including docking analysis, writing, editing, and conceptualized. K.M. performed peptide docking analysis. The manuscript was thoroughly revised and approved by both authors.

Notes

The authors declare no competing financial interest.

■ REFERENCES

(1) Zamboni, V.; Jones, R.; Umbach, A.; Ammoni, A.; Passafaro, M.; Hirsch, E.; Merio, G. R. RhoGTPases in intellectual disability: From genetics to therapeutics opportunities. *Int. J. Mol. Sci.* **1821**, *2018*, 1−35.

(2) Tejada-Simon, M. V. Modulation of actin dynamics by Rac1 to target cognitive function. *J. Neurochem.* **2015**, *133*, 767−779.

(3) Wang, M.; Gallo, N. B.; Tai, Y.; Li, B.; Van Aelst, L. Oligophrenin-1 moderates behavioral responses to stress by regulating parvalbumin interneuron activity in the medial prefrontal cortex. *Neuron* **2021**, *109*, 1636−1656.e8.

(4) Karaca, E.; Harel, T.; Pehlivan, D.; Jhangiani, S. N.; Gambin, T.; Akdemir, Z. C.; Gonzaga-Jauregui, C.; Erdin, S.; Bayram, Y.; Campbell, I. M.; Hunter, J. V.; Atik, M. M.; Van Esch, H.; Yuan, B.; Wiszniewski, W.; Isikay, S.; Yesil, G.; Yuregir, O. O.; Bozdogan, S. T.; Aslan, H.; Aydin, H.; Tos, T.; Aksoy, A.; De Vivo, D. C.; Jain, P.; Geckinli, B. B.; Sezer, O.; Gul, D.; Durmaz, B.; Cogulu, O.; Ozkinay, F.; Topcu, V.; Candan, S.; Cebi, A. H.; Ikbal, M.; Gulec, E. Y.; Gezdirici, A.; Koparir, E.; Ekici, F.; Couskun, S.; Cicek, S.; Karaer, K.; Koparir, A.; Duz, M. B.; Kirat, E.; Fenercioglu, E.; Ulucan, H.; Seven, M.; Guran, T.; Elcioglu, N.; Yildirim, M. S.; Aktas, D.; Alikasifoglu, M.; Ture, M.; Yakut, T.; Overton, J. D.; Yuksel, A.; Ozen, M.; Muzny, D. M.; Adams, D. R.; Boerwinkle, E.; Chung, W. K.; Gibbs, R. A.; Lupski, J. R. Genes that affect brain structure and function identified by rare variant analyses of Mendelian neurologic disease. *Neuron* **2015**, *88*, 499−513.

(5) Price, K. M.; Wigg, K. G.; Feng, Y.; Blokland, K.; Wilkinson, M.; He, G.; Kerr, E. N.; Carter, T. C.; Guger, S. L.; Lovett, M. W.; Strug, L. J.; Barr, C. L. Genome-wide association study of word reading: Overlap with risk genes for neurodevelopmental disorders. *Genes, Brain Behav.* **2020**, *19*, No. e12648.

(6) Pourhaghighi, R.; Ash, P. E. A.; Phanse, S.; Goebels, F.; Hu, L. Z. M.; Chen, S.; Zhang, Y.; Wierbowski, S. D.; Boudeau, S.; Moutaoufik, M. T.; Malty, R. H.; Malolepsza, E.; Tsafou, K.; Nathan, A.; Cromar, G.; Guo, H.; Abdullatif, A. A.; Apicco, D. J.; Becker, L. A.; Gitler, A. D.; Pulst, S. M.; Youssef, A.; Hekman, R.; Havugimana, P. C.; White, C. A.; Blum, B. C.; Ratti, A.; Bryant, C. D.; Parkinson, J.; Lage, K.; Babu, M.; Yu, H.; Bader, G. D.; Wolozin, B.; Emili, A. BrainMap elucidates the macromolecular connectivity landscape of mammalian brain. *Cell Syst.* **2021**, *10*, 333−350.

(7) Ménétrey, J.; Perderiset, M.; Cicolari, J.; Dubois, T.; Elkhatib, N.; Khadali, F. E.; Franco, M.; Chavrier, P.; Houdusse, A. Structural basis for ARF1-mediated recruitment of ArhGAP21 to Golgi membranes. *EMBO J.* **2007**, *26*, 1953−1962.

(8) Dubois, T.; Paléotti, O.; Mironov, A. A., Jr.; Fraisier, V.; Stradal, T. E. B.; De Matteis, M. A.; Franco, N.; Chavrier, P. Golgi-localized GAP for Cdc42 functions downstream of Arf1 to control Arp2/3 complex and F-actin dynamics. *Nat. Cell Biol.* **2005**, *7*, 353−364.

(9) Anthony, D. F.; Sin, Y. Y.; Vadrevu, S.; Advant, N.; Day, J. P.; Byrne, A. M.; Lynch, M. J.; Milligan, G.; Houslay, M. D.; Baillie, G. S. β-arrestin 1 inhibits the GTPase-activating protein function of ArhGAP21, promoting activation of RhoA following Angiotensin II type 1A receptor stimulation. *Mol. Cell. Biol.* **2011**, *31*, 1066−1075.

(10) Zhang, L.; Luga, V.; Armitage, S. K.; Musiol, M.; Won, A.; Yip, C. M.; Plotnikov, S. V.; Wrana, J. L. A lateral signalling pathway coordinates shape volatility during cell migration. *Nat. Commun.* **2016**, *7*, 11714.

(11) Xavier-Ferrucio, J.; Ricon, L.; Vieira, K.; Longhini, A. L.; Lazarini, M.; Bigarella, C. L.; Franchi, G., Jr.; Krause, D. S.; Saad, S. T. O. Hematopoietic defects in response to reduced ArhGAP21. *Stem Cell Res.* **2018**, *26*, 17−27.

(12) Pissarra, M. F.; Torello, C. O.; Gomes, R. G. B.; Shiraishi, R. N.; Santos, I.; Ferro, K. P. V.; Lopes, M. R.; Favaro, P. M. B.; Saad, S. T. O.; Lazarini, M. ArhGAP21 deficiency results in increase of osteoblastic lineage cells in the murine bone marrow microenvironment. *Front. Cell Cev. Biol.* **2021**, *9*, 3364.

(13) Katoh, M.; Katoh, M. Identification and characterization of human ArhGAP23 gene *in silico*. *Int. J. Oncol.* **2004**, *25*, 535−540.
(14) van Gelder, C. A. G. H.; Penning, R.; Veth, T. S.; Catsburg, L. A. E.; Hoogenraad, C. C.; MacGilavry, H. D.; Altelaar, M. Temporal quantitative proteomics of mGluR-induced protein translation and phosphorylation in neurons. *Mol. Cell. Proteomics* **2020**, *19*, 1952−1968.
(15) Li, J.; Zhang, W.; Yang, H.; Howrigan, D. P.; Wilkinson, B.; Souaiaia, T.; Evgrafov, O. V.; Genovese, G.; Clementel, V. A.; Tudor, J. C.; Abel, T.; Knowles, J. A.; Neale, B. M.; Wang, K.; Sun, F.; Coba, M. P. Spatio-temporal profile of postsynaptic interactomes integrates components of complex brain disorders. *Nat. Neurosci.* **2017**, *20*, 1150−1161.
(16) Martin-Vilchez, S.; Whitmore, L.; Asmussen, H.; Zareno, J.; Horwitz, R.; Newell-Litwa, K. RhoGTPase regulators orchestrate distinct stages of synaptic development. *PLoS One* **2017**, DOI: 10.1371/journal.pone.0170464.
(17) Quinlan, M. A.; Robson, M. J.; Ye, R.; Rose, K. L.; Schey, K. L.; Blakely, R. D. *Ex vivo* quantitative proteomic analysis of serotonin transporter interactome: network impact of the SERT Ala56 coding variant. *Front. Mol. Neurosci.* **2020**, *13*, 89.
(18) Wilkinson, B.; Li, J.; Coba, M. P. Synaptic GAP and GEF complexes cluster proteins essential for GTP signaling. *Sci. Rep.* **2017**, *7*, 1−12.
(19) Norden, P. R.; Sabine, A.; Wang, Y.; Demir, C. S.; Liu, T.; Petrova, T. V.; Kume, T. Shear stimulation of Foxc1 and Foxc2 differentially regulates cytoskeletal activity during lymphatic valve maturation. *eLife* **2020**, *9*, No. e53814.
(20) Amin, E.; Jaiswal, M.; Derewenda, U.; Rels, K.; Nouri, K.; Koessmeier, K. T.; Aspenström, P.; Somlyo, A. V.; Dvorsky, R.; Ahmadian, M. R. Deciphering the molecular and functional basis of RhoGAP family proteins. *J. Biol. Chem.* **2016**, *291*, 20353−20371.
(21) Jumper, J.; Evans, R.; Pritzel, A.; Green, T.; Figurnov, M.; Ronneberger, O.; Tunyasuvunakool, K.; Bates, R.; Žídek, A.; Potapenko, A.; Bridgland, A.; Meyer, C.; Kohl, S. A. A.; Ballard, A. J.; Cowie, A.; Romera-Paredes, B.; Nikolov, S.; Jain, R.; Adler, J.; Back, T.; Petersen, S.; Reiman, D.; Clancy, E.; Zielinski, M.; Steinegger, M.; Pacholska, M.; Berghammer, T.; Bodenstein, S.; Silver, D.; Vinyals, O.; Senior, A. W.; Kavukcuoglu, K.; Kohli, P.; Hassabis, D. Highly accurate protein structure prediction with AlphaFold. *Nature* **2021**, *596*, 583−589.
(22) Söding, J.; Biegert, A.; Lupas, A. N. The HHpred interactive server for protein homology detection and structure prediction. *Nucleic Acids Res.* **2005**, *33*, W244−W248.
(23) Schwede, T.; Kopp, J.; Guex, N.; Peitsch, M. C. SWISS-MODEL: an automated protein homology-modeling server. *Nucleic Acids Res.* **2003**, *31*, 3381−3385.
(24) Roy, A.; Kucukural, A.; Zhang, Y. I-TASSER: a unified platform for automated protein structure and function prediction. *Nat. Protoc.* **2010**, *5*, 725−738.
(25) Yang, J.; Anishchenko, I.; Park, H.; Peng, Z.; Ovchinnikov, S.; Baker, D. Improved protein structure prediction using predicted interresidue orientations. *Proc. Natl. Acad. Sci.* **2020**, *117*, 1496−1503.
(26) Benkert, P.; Künzli, M.; Schwede, T. QMEAN server for protein model quality estimation. *Nucleic Acids Res.* **2009**, *37*, W510−W514.
(27) Messaoudi, A.; Belguith, H.; Hamida, J. B. Homology modeling and virtual screening approaches to identify potent inhibitors of VEB-1 β-lactamase. *Theor. Biol. Med. Modell.* **2013**, *10*, 1−10.
(28) Eisenberg, D.; Lüthy, R.; Bowie, J. U. VERIFY3D: Assessment of protein models with three-dimensional profiles. *Methods Enzymol.* **1997**, *277*, 396−404.
(29) Wiederstein, M.; Sippl, M. J. ProSA-web: interactive web service for the recognition of errors in three-dimensional structures of proteins. *Nucleic Acids Res.* **2007**, *35*, W407−W410.
(30) Blum, M.; Chang, H. Y.; Chuguransky, S.; Grego, T.; Kandasaamy, S.; Mitchell, A.; Nuka, G.; Paysan-Lafosse, T.; Qureshi, M.; Raj, S.; Richardson, L.; Salazar, G. A.; Wiliams, L.; Bork, P.; Bridge, A.; Gough, J.; Haft, D. H.; Letunic, I.; Marchler-Bauer, A.; Mi, H.; Natale, D. A.; Necci, M.; Orengo, C. A.; Pandurangan, A. P.; Riboire, C.; Sigrist, C. J. A.; Sillitoe, I.; Thanki, N.; Thomas, P. D.; Tosatto, S. C. E.; Wu, C. H.; Bateman, A.; Finn, R. D. The InterPro protein families and domain database: 20 years on. *Nucleic Acids Res.* **2021**, *49*, D344−D354.
(31) Buchan, D. W. A.; Minneci, F.; Nugent, T. C. O.; Bryson, K.; Jones, D. T. Scalable web services for the PSIPRED protein analysis workbench. *Nucleic Acids Res.* **2013**, *41*, W349−W357.
(32) Katoh, K.; Rozewicki, J.; Yamada, K. D. MAFFT online service: multiple sequence alignment interactive sequence choice and visualization. *Briefings in Bioinformatics* **2019**, *20*, 1160−1166.
(33) Yan, Y.; Zhang, D.; Zhou, P.; Li, B.; Huang, S. Y. HDOCK: a web server for protein-protein and protein-DNA/RNA docking based on a hybrid strategy. *Nucleic Acids Res.* **2017**, *45*, W365−W373.
(34) van Zundert, G. C. P.; Rodrigues, J. P. G. L. M.; Trellet, M.; Schmitz, C.; Kastritis, P. L.; Karaca, E.; Melquiond, A. S. J.; van Dijk, M.; de Vries, S. J.; Bonvin, A. M. J. J. The HADDOCK2.2 web server: User-friendly integrative modeling of biomolecular complexes. *J. Mol. Biol.* **2016**, *428*, 720−725.
(35) Pokala, N.; Handel, T. M. Energy functions for protein design: Adjustment with protein-protein complex affinities, models for the unfolded state, and negative design of solubility and specificity. *J. Mol. Biol.* **2005**, *347*, 203−227.
(36) Krüger, D. M.; Gohlke, H. DrugScore^{PPI} webserver: fast and accurate *in silico* alanine scanning for scoring protein-protein interactions. *Nucleic Acids Res.* **2010**, *38*, W480−W486.
(37) Xue, L. C.; Rodrigues, J. P.; Kastritis, P. L.; Bonvin, A. M.; Vangone, A. PRODIGY: a web server for predicting the binding affinity of protein-protein complexes. *Bioinformatics* **2016**, *32*, 3676−3678.
(38) Vangone, A.; Bonvin, A. M. J. J. Contacts-based prediction of binding affinity in protein-protein complexes. *eLIFE* **2015**, *4*, No. e07454.
(39) Chatr-aryamontri, A.; Breitkreutz, B. J.; Oughtred, R.; Boucher, L.; Heinicke, S.; Chen, D.; Stark, C.; Breitkreutz, A.; Kolas, N.; O'Donnell, L.; Reguly, T.; Nixon, J.; Ramage, L.; Winter, A.; Sellam, A.; Chang, C.; Hirschman, J.; Theesfeld, C.; Rust, J.; Livstone, M. S.; Dolinski, K.; Tyers, M. The BioGRID interaction database: 2015 update. *Nucleic Acids Res.* **2015**, *43*, D470−D478.
(40) Orchard, S.; Ammari, M.; Aranda, B.; Breuza, L.; Briganti, L.; Broackes-Carter, F.; Campbell, N. H.; Chavali, G.; Chen, C.; del-Toro, N.; Duesbury, M.; Dumousseau, M.; Galeota, E.; Hinz, U.; Iannuccelli, M.; Jagannathan, S.; Jimenez, R.; Khadake, J.; Lagreid, A.; Licata, L.; Lovering, R. C.; Meldal, B.; Melidoni, A. N.; Milagros, M.; Peluso, D.; Perfetto, L.; Porras, P.; Raghunath, A.; Ricard-Blum, S.; Roechert, B.; Stutz, A.; Tognolli, M.; van Roey, K.; Cesareni, G.; Hermjakob, H. The MIntAct project − IntAct as a common curation platform for 11 molecular interaction databases. *Nucleic Acids Res.* **2015**, *42*, D358−D363.
(41) Müller, P. M.; Rademacher, J.; Bagshaw, R. D.; Wortmann, C.; Barth, C.; van Unen, J.; Alp, K. M.; Giudice, G.; Eccles, R. L.; Heinrich, L. E.; Pascual-Vargas, P.; Sanchez-Castro, M.; Brandenburg, L.; Mbamalu, G.; Tucholska, M.; Spatt, L.; Czajkowski, M. T.; Welke, R. W.; Zhang, S.; Nguyen, V.; Rrustemi, T.; Trnka, P.; Freitag, K.; Larsen, B.; Popp, O.; Mertins, P.; Gingras, A. C.; Roth, F. P.; Colwill, K.; Bakal, C.; Pertz, O.; Pawson, T.; Petsalaki, E.; Rocks, O. Systems analysis of RhoGEF and RhoGAP regulatory proteins reveals spatially organized Rac1 signaling from integrin adhesions. *Nat. Cell Biol.* **2020**, *22*, 498−511.
(42) Bagci, H.; Sriskandarajah, N.; Robert, A.; Boulais, J.; Elkholi, I. E.; Tran, V.; Lin, Z. Y.; Thibault, M. P.; Dubé, N.; Faubert, D.; Hipfner, D. R.; Gingras, A. C.; Côté, J. F. Mapping the proximity interaction network of the Rho-family GTPases reveals signaling pathways and regulatory mechanisms. *Nat. Cell Biol.* **2020**, *22*, 120−134.
(43) Mishima, M.; Glotzer, M. Cytokinesis: A logical GAP. *Curr. Biol.* **2003**, *13*, R589−R591.
(44) Bao, H.; Li, F.; Wang, C.; Wang, N.; Jiang, Y.; Tang, Y.; Wu, J.; Shi, Y. Structural basis for the specific recognition of RhoA by the

dual GTPase-activating protein ARAP3. *J. Biol. Chem.* **2016**, *291*, 16709−16719.
(45) Graham, D. L.; Eccleston, J. F.; Lowe, P. N. The conserved arginine in Rho-GTPase-activating protein is essential for efficient catalysis but not for complex formation with Rho-GDP and aluminum fluoride. *Biochemistry* **1999**, *38*, 985−991.
(46) Jelen, F.; Lachowicz, P.; Apostoluk, W.; Mateja, A.; Derewenda, Z. S.; Otlewski, J. Dissecting the thermodynamics of GAP-RhoA interactions. *J. Struct. Biol.* **2009**, *165*, 10−18.
(47) Jaiswal, M.; Dvorsky, R.; Ahmadian, M. R. Functional cross-talk between Ras and Rho pathways. *J. Biol. Chem.* **2014**, *289*, 6839−6849.
(48) Lazarini, M.; Traina, F.; Machado-Neto, J. A.; Barcellos, K. S. A.; Moreira, Y. B.; Brandão, M. M.; Verjovski-Almeida, S.; Ridley, A. J.; Saad, S. T. O. ArhGAP21 is a RhoGAP for RhoA and RhoC with a role in proliferation and migration of prostate adenocarcinoma cells. *Biochim. Biophys. Acta* **2013**, *1832*, 365−374.
(49) Kumari, S.; Mayor, S. Arf1 is directly involved in dynamin-independent endocytosis. *Nat. Cell Biol.* **2008**, *10*, 30−41.
(50) Elkins, J. M.; Gileadi, C.; Shrestha, L.; Phillips, C.; Wang, J.; Muniz, J. R. C.; Doyle, D. A. Unusual binding insteractions in PDZ domain crystal structures help explain binding mechanisms. *Protein Sci.* **2010**, *19*, 731−741.
(51) Javadi, A.; Deevi, R. K.; Evergren, E.; Blondel-Tepaz, E.; Baillie, G. S.; Scott, M. G. H.; Campbell, F. C. PTEN controls glandular morphogenesis through a juxtamembrane β- arrestin1/ArhGAP21 scaffolding complex. *eLIFE* **2017**, *6*, No. e24578.
(52) Xiao, K.; McClatchy, D. B.; Shukla, A. K.; Zhao, Y.; Chen, M.; Shenoy, S. K.; Yates, J. R., III; Lefkowitz, R. J. Functional specialization of β-arrestin interactions revealed by proteomic analysis. *Proc. Natl. Acad. Sci.* **2007**, *29*, 12011−12016.
(53) Terrien, E.; Chaffotte, A.; Lafage, M.; Khan, Z.; Préhaud, C.; Cordier, F.; Simenel, C.; Delepierre, M.; Buc, H.; Lafon, M.; Wolff, N. Intereference with the PTEN-MAST2 interaction by a viral protein leads to cellular relocalization of PTEN. *Sci. Signaling* **2012**, *5*, ra58.
(54) Macia, E.; Partisani, M.; Favard, C.; Mortier, E.; Zimmermann, P.; Carlier, M. F.; Gounon, P.; Luton, F.; Franco, M. The pleckstrin homology domain of the Arf6-specific exchange factor EFA6 localizes to the plasma membrane by interacting with phosphatidylinositol 4,5-bisphosphate and F-actin. *J. Biol. Chem.* **2008**, *283*, 19836−19844.
(55) Ketschek, K. A.; Gallo, G. Nerve growth factor induces axonal filopodia through localized microdomains of phosphoinositide 3-kinase activity that drive the formation of cytoskeletal precursors to filopodia. *J. Neurosci.* **2010**, *30*, 12185−12197.
(56) Cuesto, G.; Enriquez-Barreto, L.; Caramés, C.; Cantarero, M.; Gasull, X.; Sandi, C.; Ferrús, A.; Acebes, A.; Morales, M. Phosphoinositide 3-kinase activation controls synaptogenesis and spinogenesis in hippocampal neurons. *J. Neurosci.* **2011**, *31*, 2721−2733.
(57) Gibson, T. J.; Dinkel, H.; Roey, K. V.; Diella, F. Experimental detection of short regulatory motifs in eukaryotic proteins: tips for good practice as well as for bad. *Cell Commun. Signal.* **2015**, *13*, 1−15.
(58) Dinkel, H.; Roey, K. V.; Michael, S.; Kumar, M.; Uyar, B.; Altenberg, B.; Milchevskaya, V.; Schneider, M.; Kühn, H.; Behrendt, A.; Dahl, S. L.; Damerell, V.; Diebel, S.; Kalman, S.; Klein, S.; Knudsen, A. C.; Mäder, C.; Merrill, S.; Staudt, A.; Thiel, V.; Welti, L.; Davey, N. E.; Diella, F.; Gibson, T. J. ELM 2016- data update and new functionality of eukaryotic linear motif resource. *Nucleic Acids Res.* **2016**, *44*, D293−D300.
(59) Kouchi, Z.; Kojima, M. Function of SYDE C2-RhoGAP family as signaling hubs for neuronal development deduced by computational analysis. *Sci. Rep.* **2022**, *12*, 4325.
(60) Dinkel, H.; Van Roey, K.; Michael, S.; Kumar, M.; Uyar, B.; Altenberg, B.; Milchevskaya, V.; Schneider, M.; Kühn, H.; Behrendt, A.; Dahl, S. L.; Damerell, V.; Diebel, S.; Kalman, S.; Klein, S.; Knudsen, A. C.; Mäder, C.; Merrill, S.; Staudt, A.; Thiel, V.; Welti, L.; Davey, N. E.; Diella, F.; Gibson, T. J. ELM-2016 − data update and new functionality of eukaryote linear motif resource. *Nucleic Acids Res.* **2016**, *44*, D294−D300.
(61) Oates, M. E.; Romero, P.; Ishida, T.; Ghalwash, M.; Mizianty, M. J.; Xue, B.; Dosztányi, Z.; Uversky, V. N.; Obradovic, Z.; Kurgan, L.; Dunker, A. K.; Gough, J. D^2P^2: database of disordered protein predictions. *Nucleic Acids Res.* **2012**, *41*, D508−D516.
(62) Potenza, E.; Di Domenico, T.; Walsh, I.; Tosatto, S. C. E. MobiDB 2.0: an improved database of intrinsically disordered and mobile proteins. *Nucleic Acid. Res.* **2015**, *43*, D315−D320.
(63) Meek, S. E. M.; Lane, W. S.; Piwnica-Worms, H. Comprehensive proteomic analysis of interphase and mitotic 14-3-3-binding proteins. *J. Biol. Chem.* **2004**, *279*, 32046−32054.
(64) Benzinger, A.; Muster, N.; Koch, H. B.; Yates, J. R., III; Hermeking, H. Targeted proteomic analysis of 14-3-3σ, a p53 effector commonly silenced in cancer. *Mol. Cell. Proteomics* **2005**, *4*, 785−795.
(65) Ichimura, T.; Taoka, M.; Shoji, I.; Kato, H.; Sato, T.; Hatakeyama, S.; Isobe, T.; Hachiya, N. 14-3-3 proteins sequester a pool of soluble TRIM32 ubiquitin ligase to repress autoubiquitylation and cytoplasmic body formation. *J. Cell Sci.* **2015**, *126*, 2014−2026.
(66) Johnson, C.; Crowther, S.; Stafford, M. J.; Campbell, D. G.; Toth, R.; Mackintosh, C. Bioinformatic and experimental survey of 14-3-3-binding sites. *Biochem. J.* **2010**, *427*, 69−78.
(67) Hamdan, H.; Lim, B. C.; Torii, T.; Joshi, A.; Konning, M.; Smith, C.; Palmer, D. J.; Ng, P.; Leterrier, C.; Oses-Pieto, J. A.; Burlingame, A. L.; Rasband, M. N. Mapping axon initial segment structure and function by multiplexed proximity biotinylation. *Nat. Commun.* **2020**, *11*, 1−17.
(68) Bréchet, A.; Fache, M. P.; Brachet, A.; Ferracci, G.; Baude, A.; Irondelle, M.; Pereira, S.; Leterrier, C.; Dargent, B. Protein kinase CK2 contributes to the organization of sodium channels in axonal membranes by regulating their interactions with ankyrin G. *J. Cell Biol.* **2008**, *183*, 1101−1114.
(69) Xu, M.; Cooper, E. C. An ankyrin-G N-terminal gate and protein kinase CK2 dually regulate binding of voltage-gated sodium and KCNQ2/3 potassium channels. *J. Biol. Chem.* **2015**, *290*, 16619−16632.
(70) Iqbal, Z.; Vandeweyer, G.; van der Voet, M.; Waryah, A. M.; Zahoor, M. Y.; Besseling, J. A.; Roca, L. T.; Silfhout, A. T. V.; Nijhof, B.; Kramer, J. M.; Van der Aa, N.; Ansar, M.; Peeters, H.; Helsmoortel, C.; Gilissen, C.; Vissers, L. E. L. M.; Veltman, J. A.; de Brouwer, A. P. M.; Kooy, R. F.; Riazuddin, S.; Schenck, A.; van Bokhoven, H.; Rooms, L. Homozygous and heterozygous disruption of Ank3: at the crossroads of neurodevelopmental psychiatric disorders. *Hum. Mol. Genet.* **2013**, *22*, 1960−1970.
(71) Sakamoto, M.; Sasaki, K.; Sugie, A.; Nitta, Y.; Kimura, T.; Gürsoy, S.; Cinleti, T.; Iai, M.; Sengoku, T.; Ogata, K.; Suzuki, A.; Okamoto, N.; Iwama, K.; Tsuchida, N.; Uchimura, Y.; Koshimizu, E.; Fujita, A.; Hamanaka, K.; Miyatake, S.; Mizuguchi, T.; Taguri, M.; Ito, S.; Takahashi, H.; Miyake, N.; Matsumoto, N. *De novo ARF3* variants cause neurodevelopmental disorder with brain abnormality. *Hum. Mol. Genet.* **2021**, *31*, 69−81.
(72) Koutras, C.; Lévesque, G. Identification of novel NPRAP/δ-catenin-interacting proteins and the direct association of NRRAP with dynamin2. *PLoS One* **2011**, *10*, No. e25379.
(73) Kim, H.; Han, J. R.; Park, J.; Oh, M.; James, S. E.; Chang, S.; Lu, Q.; Lee, K. Y.; Ki, H.; Song, J. W.; Kim, K. δ-catenin-induced dendritic morphogenesis. An essential role of p190RhoGEF interaction through Akt1-mediated phosphorylation. *J. Biol. Chem.* **2008**, *283*, 977−987.
(74) Galisteo, M. L.; Yang, Y.; Urena, J.; Schlessinger, J. Activation of the nonreceptor protein tyrosine kinase Ack by multiple extracellular stimuli. *Proc. Natl. Acad. Sci.* **2006**, *103*, 9796−9801.
(75) del Mar Masdeu, M.; Armendáriz, B. G.; La Torre, A.; Soriano, E.; Burgaya, F.; Ureña, J. M. Identification of novel Ack1-interacting proteins and Ack1 phosphorylated sites in mouse brain by mass spectrometry. *Oncotarget* **2017**, *8*, 101146−101157.
(76) Lee, S. E.; Kim, J. A.; Chang, S. nArgBP2-SAPAP-SHANK, the core postsynaptic triad associated with psychiatric disorders. *Exp. Mol. Med.* **2018**, *50*, 1−9.
(77) Tao, J.; Wu, H.; Coronado, A. A.; de Laittre, E.; Osterweil, E. K.; Zhang, Y.; Bear, M. F. Negative allosteric modulation of mGluR5

https://doi.org/10.1021/acsomega.2c08054
ACS Omega 2023, 8, 19249−19264

partially corrects pathophysiology in a mouse model of Rett syndrome. *J. Neurosci.* **2016**, *36*, 11946−11958.
(78) Nehru, V.; Voytyuk, O.; Lennartsson, J.; Aspenström, P. RhoD binds the Rab5 effector rabankyrin-5 and has a role in trafficking of platelet-derived growth factor receptor. *Traffic* **2013**, *14*, 1242−1254.
(79) Jovanovic, O. A.; Brown, F. D.; Donaldson, J. G. An effector domain mutant of Arf6 implicates phospholipase D in endosomal membrane recycling. *Mol. Biol. Cell* **2006**, *17*, 327−335.
(80) Tagliatti, E.; Fadda, M.; Falace, A.; Benfenati, F.; Fassio, A. Arf6 regulates the cycling and the readily releasable pool of synaptic vesicles at hippocampal synapse. *eLife* **2016**, *5*, No. e10116.
(81) Gad, A. K. B.; Nehru, V.; Ruusala, A.; Aspenström, P. RhoD regulates cytoskeletal dynamics via the actin-nucleation-promoting factor WASp homologue associated with actin Golgi membranes and microtubules. *Mol. Biol. Cell* **2012**, *23*, 4807−4819.
(82) Barcellos, K. S. A.; Bigarella, C. L.; Wagner, M. V.; Vieira, K. P.; Lazarini, M.; Langford, P. R.; Machado-Neto, J. A.; Call, S. G.; Staley, D. M.; Chung, J. Y.; Hansen, M. D.; Saad, S. T. O. ArhGAP21 protein, a new partner of α-tubulin involved in cell-cell adhesion formation and essential for epithelial-mesenchymal transition. *J. Biol. Chem.* **2013**, *288*, 2179−2189.
(83) Bigarella, C. L.; Borges, L.; Costa, F. F.; Terezinha, S.; Saad, O. ArhGAP21 modulates FAK activity and impairs glioblastoma cell migration. *Biochim. Biophys. Acta* **2009**, *1793*, 806−816.
(84) Hildebrand, J. D.; Taylor, J. M.; Parsons, T. An SH3 domain-containing GTPase-activating protein for Rho and Cdc42 associates with focal adhesion kinase. *Mol. Cell. Biol.* **1996**, *16*, 3169−3178.
(85) McNair, K.; Spike, R.; Guilding, C.; Prendergast, G. C. P.; Stone, T. W.; Cobb, S. R.; Morris, B. J. A role for RhoB in synaptic plasticity and the regulation of neuronal morphology. *J. Neurosci.* **2010**, *30*, 3508−3517.
(86) Sandilands, E.; Cans, C.; Fincham, V. J.; Brunton, V. G.; Mellor, H.; Prendergast, G. C.; Norman, J. C.; Superti-Furga, G.; Frame, M. C. RhoB and actin polymerization coordinate Src activation with endosome-mediated delivery to the membrane. *Dev. Cell* **2004**, *7*, 855−869.
(87) Fujita, A.; Koinuma, S.; Yasuda, S.; Nagai, H.; Kamiguchi, H.; Wada, N.; Nakamura, T. GTP hydrolysis of TC10 promotes neurite outgrowth through exocytic fusion of rab11- and L1-containing vesicles by releasing exocyst component Exo70. *PLoS One* **2013**, *8*, No. e79689.
(88) Tian, D.; Diao, M.; Jiang, Y.; Sun, L.; Zhang, Y.; Chen, Z.; Huang, S.; Ou, G. Anillin regulates neuronal migration and neurite growth by linking RhoG to the actin cytoskeleton. *Curr. Biol.* **2015**, *25*, 1135−1145.
(89) Delhommel, F.; Chaffotte, A.; Terrien, E.; Raynal, B.; Buc, H.; Delepierre, M.; Cordier, F.; Wolff, N. Deciphering the unconventional peptide binding to the PDZ domain of MAST2. *Biochem. J.* **2015**, *469*, 159−168.

https://doi.org/10.1021/acsomega.2c08054
ACS Omega 2023, 8, 19249−19264